Derivation of Trajectory Predictor Input Distributions from Observed Data

Rudnyk, Julia; Ellerbroek, Joost; Hoekstra, Jacco

DOI
10.2514/6.2018-3354

Publication date
2018

Document Version
Accepted author manuscript

Published in
2018 Aviation Technology, Integration, and Operations Conference

Derivation of Trajectory Predictor Input Distributions from Observed Data

Julia Rudnyk*, Joost Ellerbroek†, and Jacco M. Hoekstra‡
Control and Simulation, Faculty of Aerospace Engineering,
Delft University of Technology, Delft, the Netherlands

Trajectory predictor performance is dependent on input data quality, which is usually far from perfect. Whereas previous research has mostly focused on mathematical models used for the trajectory prediction and errors present in the prediction process, the comparison of common assumptions made about input values with observed (real) data has not received much attention. In this paper, probability distribution functions are obtained per aircraft wake turbulence category for a set of inputs to a trajectory predictor based on observed data. Considered inputs include aircraft bank angle, indicated airspeed and Mach number speed profiles, vertical speed, temporary level-offs in climb and descent, air temperature, wind speed and wind direction, and air traffic control instructions. Surveillance data, weather forecasts, and air traffic controllers' inputs are used as the data source. Obtained distributions are compared with common simplified assumptions and their characteristics are addressed. The results of this study could be used to improve trajectory prediction.

I. Introduction

TRAJECTORY prediction is an important part of most decision support tools that assist Air Traffic Controllers (ATCos) in their current, day to day operations. Medium Term Conflict Detection (MTCD) uses the combination of two predicted trajectories, which increases the sensitivity to inaccuracies. In addition, the proposed concept of Trajectory Based Operations is also based on trajectory prediction [1, 2]. Several of these decision support tools require high accuracy predictions, which is a challenge under the presence of numerous uncertainties related to trajectory predictor input data. Whereas prior research studied different mathematical models used in trajectory predictors [3] and sources of errors present in the prediction process [4], little effort has been made to compare the common assumptions about the trajectory predictors' input values with real observed data. Although it is commonly agreed that the input data quality is vital for accurate trajectory predictions, often the description of inputs is simplified for convenience.

The aim of this study is to broaden current knowledge of trajectory predictors inputs' values by deriving the distributions of the inputs and comparing them with assumptions commonly made. The input parameters were selected for this study based on previous research [4–11] and include the aircraft bank angle, the indicated airspeed (IAS)/Mach number speed profiles, the vertical speed, the temporary level-offs, the outside air temperature, the wind speed and direction. Although previous research has not looked at Air Traffic Control (ATC) instructions as one of the inputs, it was included in this study and considered to be an important input to a trajectory predictor.

In literature, there is a great deal of variability in how trajectory predictor input values are selected and specified (see Table 7 of the Appendix A for an input value settings' summary). Values can, for instance, be assumed based on common knowledge; they can be estimated from flight data; they can be based on an aircraft performance model, such as BADA [12], or documents like Flight Crew Operations Manual [13]. In case of bank angle settings, sometimes nominal [12, 14] or maximum values are used [5, 12], whereas other studies only reported using 'constant' bank angles, without stating their values [15, 16].

Despite aircraft speed settings being calculated based on the cost index selected for each individual flight, a single-speed profile is commonly assumed per aircraft type [12, 17]. To model the observed speed variability [18, 19], sometimes a set of speed profiles is used [4, 20], whereas in other cases a uniform [21, 22], triangular [23] or normal [22] distributions are assumed. Although vertical speed is rarely used as a trajectory predictor input (i.e. often it is the result of the selected speed settings and climb/descent angle), the knowledge of its variability [17, 24, 25] could be used to ensure a reasonable performance of the prediction model (e.g. for maximum vertical speed for passengers' comfort).

*PhD candidate, Control and Simulation, Faculty of Aerospace Engineering, Delft University of Technology, the Netherlands
†Assistant Professor, Control and Simulation, Faculty of Aerospace Engineering, Delft University of Technology, the Netherlands
‡Professor, Control and Simulation, Faculty of Aerospace Engineering, Delft University of Technology, the Netherlands, AIAA Member

Barring a few exceptions [4, 5, 8], studies on trajectory prediction seldom incorporate temporary level-offs when modeling a vertical profile. According to various studies, level-offs occur in 14% to 28% of the climbs [4, 5, 26–28], and in 42% to 64% of the descents [26, 28]. It should be noted, though, that temporary level-offs are mainly the result of ATC instructions, which implies that their frequency, duration and level-off altitude depend on the complexity of airspace geometry and traffic. Nevertheless, their non-negligible frequency indicates the necessity to include them in the trajectory prediction process if available. Commonly, ATC instructions or ATC intent is not considered as one of the trajectory predictor inputs and therefore, is not modeled.

When modeling atmospheric conditions, often International Standard Atmosphere (ISA) conditions, such as ICAO ISA [29], are assumed, although it has been shown that deviations from the standard atmosphere are commonplace [30]. The most common way to model a non-standard atmosphere is by using a fixed temperature offset (e.g. ISA±10 degrees). Alternatives, for instance, are to use a uniform distribution of a temperature offset [21]. Horizontal wind is often assumed to be zero or modeled using nominal and stochastic wind components [14, 31, 32], whereas vertical wind profiles are implemented as linearly increasing with altitude [33]. Sometimes, wind is modeled using a uniform [34] or normal [35] distribution. Nevertheless, real-life wind distributions do not seem to follow these distributions [36]. Another approach to model weather variability employs forecast ensembles [22], which can be obtained from a weather forecast provider. Usually, forecast ensembles are computationally expensive and all forecasts within an ensemble are equally likely.

Most previous research on trajectory prediction employs a simplified approach to define inputs to a trajectory predictor as a single setting or a range of feasible values, which is not representative for real operations. Although some studies did model inputs using probability distribution functions, most of those functions and their parameters were based on assumptions and not on observed data.

The objective of this paper is therefore to derive probability distribution functions for selected input factors based on observed data. In this way, the variability of the inputs can be expressed with a higher level of accuracy and less uncertainty. This could lead to more realistic predictions and hence improve the performance of decision support tools. In this study, most of the distribution functions will be estimated per wake turbulence category. Where applicable, two types of distribution functions are given: non-parametric (kernel-density estimate) and parametric (best fit from known theoretical distributions) and common (simplified) assumptions about some factors are discussed.

II. Methodology

A. Probability Distribution Function

Each studied parameter is considered as a random variable and the goal is to describe it using a probability function or a set of such functions. The latter is applicable to parameters, which require two or more characteristics to be defined (e.g. temporary level-offs are characterized by the flight level at which they occur and their duration) or whose distribution is a function of a certain parameter (e.g. vertical speed distribution depends on altitude).

Although the majority of studied parameters can be represented as continuous random variables, some parameters (e.g., the flight level of a temporary level-off) should be characterized as discrete random variables. A continuous random variable is described by a probability density function (PDF) f, while a discrete random variable is described by a probability mass function (PMF) p. The probability P that a continuous random variable X takes on a particular value x is 0 and, instead, the probability that X falls within a range from a to b is found:

$$P(a \leq X \leq b) = \int_a^b f(x)dx \tag{1}$$

The PDF f is the derivative of the cumulative distribution function $F(x)$. The probability P that a discrete random variable X takes on a particular value x is

$$P(X = x) = p(x) \tag{2}$$

B. Maximum Likelihood Estimate

The estimation of the distributions of the studied parameters is a two-step process, which consists of the estimation of the distribution parameters (this subsection) and evaluation of the goodness of fit (next subsection).

Unknown parameters of a distribution can be estimated from the observations by means of a maximum likelihood estimation (MLE) [37]. MLE finds such values of parameters, which make the observed data most probable, i.e. most likely. A sample $X = x_1, \ldots, x_n$ of n observations comes from a distribution f defined by a vector of parameters θ, $f(X \mid \theta)$. Assuming these observations are independent and identically distributed, their joint distribution can be expressed as:

$$f(X \mid \theta) = f(x_1, \ldots, x_n \mid \theta) = \prod_{i=1}^{n} f(x_i \mid \theta) \tag{3}$$

The likelihood $\mathcal{L}$ is a probability of obtaining observed values given certain values of parameters:

$$\mathcal{L}(\theta \mid X) = \prod_{i=1}^{n} f(x_i \mid \theta) \tag{4}$$

This can be simplified to

$$log\,\mathcal{L}(\theta \mid X) = log \prod_{i=1}^{n} f(x_i \mid \theta) = \sum_{i=1}^{n} log\, f(x_i \mid \theta) \tag{5}$$

Then, the maximum likelihood estimate of θ (θ_{MLE}) is that value of θ that maximizes $\mathcal{L}$:

$$\theta_{MLE} = \arg\max_{\theta} log\,\mathcal{L}(\theta \mid X) = \arg\max_{\theta} \sum_{i=1}^{n} log\, f(x_i \mid \theta) \tag{6}$$

In this study, parameters of PDFs were estimated using MLE.

C. Kolmogorov-Smirnov Test

After a data sample is fit to a distribution, i.e. its parameters are estimated by MLE, a Kolmogorov-Smirnov (K-S) test is performed to test the goodness of fit. The K-S test determines if a data sample comes from a population with a certain distribution [38]. The test is based on the maximum distance D (Eq. (7)), i.e. K-S statistic, between a hypothetical cumulative distribution function $F(x)$ and an empirical distribution function $F_N(x)$ obtained from the data sample. If the data sample comes from this hypothetical distribution, D should be small.

$$D = \max\left|F(x) - F_N(x)\right| \tag{7}$$

In this study, the K-S test was applied to PDFs obtained using MLE and the distribution that resulted in the smallest K-S statistic D was chosen as the best fit.

D. Kernel Density Estimate

Although it is preferable to describe the distribution of data with a parametric PDF (i.e. defined using parameters such as location, scale, and shape), this is an approximation (sometimes a very poor one if data have a complicated distribution) which could lead to an imprecise representation of probabilities of the studied parameters. A more accurate estimation of data probability is the kernel density estimation (KDE).

KDE is a non-parametric method [39], which estimates a probability density directly from data (Fig. 1) using a kernel K and a bandwidth h. A kernel is a non-negative symmetric PDF which integrates to 1 (e.g. standard normal distribution) and whose width is determined by a bandwidth h. A scaled kernel $h^{-1}K[(x - x_i)/h]$ is centered at each data point x_i, $i = 1, 2, \ldots, n$ and in a neighborhood with a high concentration of data points, these kernels pile up (Fig. 1a). The KDE $f(x)$ (Fig. 1d) is obtained by summing the scaled kernels and dividing them by n to ensure that the definite integral of $f(x)$ over its support is 1:

$$f(x) = \frac{1}{nh} \sum_{i=1}^{n} K\left(\frac{x - x_i}{h}\right) \tag{8}$$

In Eq. (8) higher weights are assigned to observations x_i that are closer to a point x. When computing a KDE, the choice of a kernel, i.e. a shape, is less important than the choice of a bandwidth. A bandwidth determines the influence

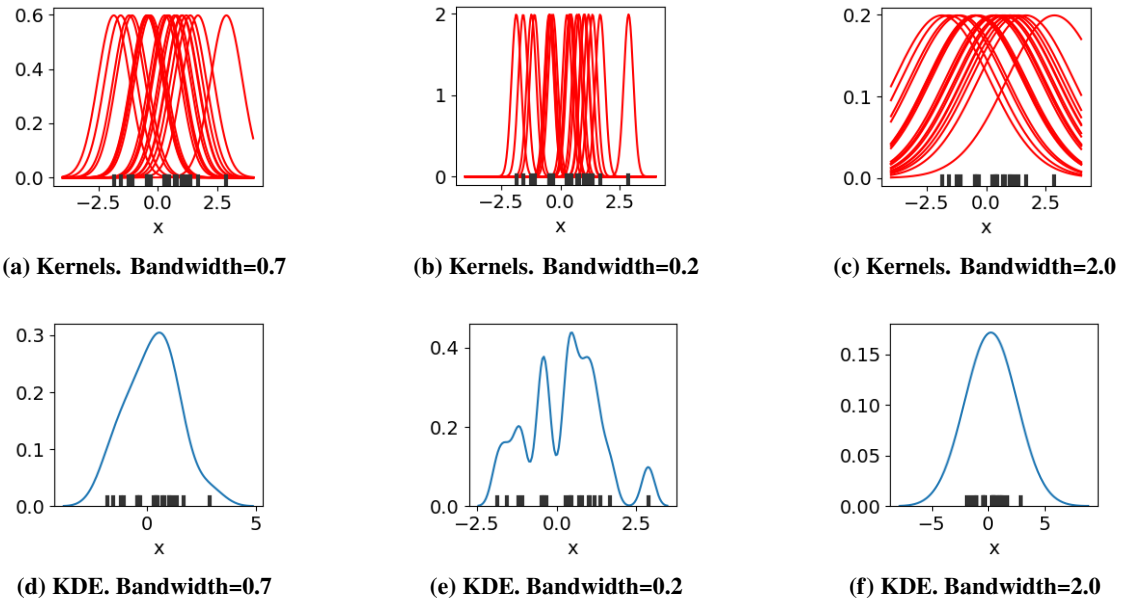

(a) Kernels. Bandwidth=0.7 **(b) Kernels. Bandwidth=0.2** **(c) Kernels. Bandwidth=2.0**

(d) KDE. Bandwidth=0.7 **(e) KDE. Bandwidth=0.2** **(f) KDE. Bandwidth=2.0**

Fig. 1 Kernel density estimate (KDE) of the data points with a Gaussian kernel of different bandwidth. Black markings indicate the data points. Red lines show the kernels of different bandwidth centered at each point. Blue lines are the resultant KDEs. The bandwidth of 0.7 is the optimal bandwidth value.

of each observation. A too narrow bandwidth (Fig. 1b) will result in a curve with too many spikes (Fig. 1e), while a too large bandwidth (Fig. 1c) will result in an over-smoothed curve (Fig. 1f).

In this study, the Gaussian kernel $N(0, 1)$ was used (Eq. (9)), while the bandwidth h was computed using Silverman's rule of thumb (Eq. (10)) [40], where s is the sample standard deviation and n is the number of data points.

$$K(u) = \frac{1}{\sqrt{2\pi}} \exp(-u^2/2) \tag{9}$$

$$h = 1.06s \cdot n^{-1/5} \tag{10}$$

E. Savitzky-Golay Filter

The acquired data for one of the studied parameters - namely speed profile - were too noisy and unsuitable to be evaluated. To smoothen data, a Savitzky-Golay filter was applied. A Savitzky-Golay filter is based on the least-squares polynomial approximation of data in a small window [41]. Using a least-squares approach, a polynomial is fit to a group of data points, i.e. window, centered at a point x. The obtained polynomial is used to estimate x, i.e. smooth the output. Then, the window is shifted forward by 1 data point, i.e. moving window, and the process is repeated. In this way, all data points are adjusted relative to the neighboring data points.

There are no exact guidelines for choosing the length of the window and the order of the polynomial. Usually, the length of the window M must be larger than the order of the polynomial N. If M is close to $N + 1$, i.e. the number of coefficients of the polynomial, the polynomial interpolates data points instead of smoothing them. Often, the window length is chosen to be an odd number and the best combination of M and N is determined by experimenting.

III. Data Used in This Study

A. Data Source

1. Surveillance Data

Surveillance data, including Mode-S information, were provided in ASTERIX Category 062 format [42] by Maastricht Upper Area Control (MUAC) and are used in this study. Figure 2 shows the MUAC airspace geographic

boundaries in blue and MUAC primary and secondary surveillance radar (further radar) coverage is indicated by the red area. Data were available over a period from 1^{st} until 7^{th} of July 2016 with update rate every 4-5 seconds. During the mentioned period meteorological conditions en-route included cumulonimbus activity, one thunderstorm and one occurrence of heavy rain. No icing, strong winds or low visibility occurred. Airspace regulations were issued by air traffic management on the 5^{th} of July due to a French strike and on the 7^{th} of July due to the Euro 2016 soccer championship and military activity. The mentioned regulations and weather conditions are considered not to have a significant impact on the statistics obtained for the studied parameters.

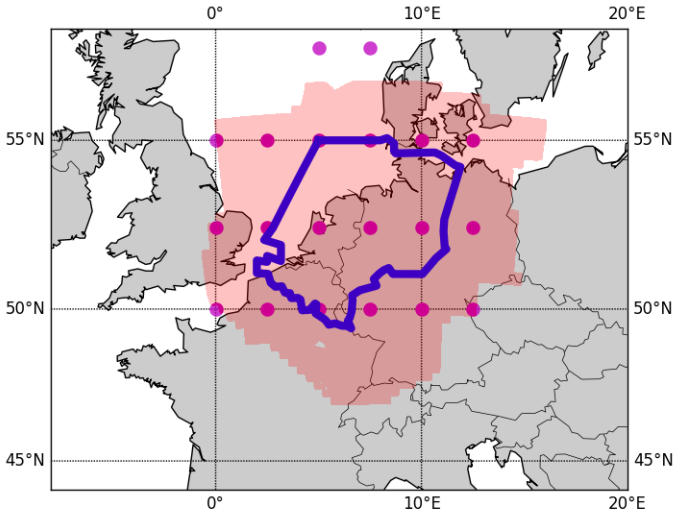

Fig. 2 MUAC airspace boundaries (blue), MUAC radar coverage (red area), weather forecast points (purple).

2. ATCo Input Data

Inputs of MUAC ATCos to a Flight Data Processing System were provided for 2016 and include, among others, 'direct', heading, speed, and climb/descend instructions.

3. Weather Forecast

Weather forecasts in MWW format are provided by the Royal Netherlands Meteorological Institute and were obtained from MUAC for 2016. Forecasts in MWW format used in this study contain wind direction, wind speed and air temperature for 20 predefined geographic locations for 10 flight levels ranging from flight level (FL) 50 to FL530. These locations are shown in Fig. 2 as purple dots.

B. Data Pre-processing

1. Flights Selection

On average, data from approximately 18,000 flights were received by MUAC radar per day and, of those, the flight plans (FPLs) of approximately 5,900 flights were sent to MUAC. Since it is not obligatory to provide information about aircraft type, wake turbulence category and flight type in Mode-S, these data were extracted from the MUAC FPL database. Therefore, only those flights for which FPLs were received by MUAC were considered in this study. Furthermore, scheduled and non-scheduled flights were analyzed. Data used in this study were not geographically and/or vertically limited to MUAC airspace, all messages within radar coverage were considered. Table 1 shows the resulting number and percentage of flights per wake turbulence category (WTC) for 7 days.

2. Data Cleaning and Flight Phase Determination

Data records which did not contain a date/time stamp, call sign, position information or altitude were filtered out and discarded. Scattered messages were ordered and organized in flights.

Table 1 Number and percentage of flights per WTC for 7 days

WTC	Flights	%
Heavy	7,143	17.4
Medium	33,113	80.7
Light	758	1.9
Total	41,014	100

In this study, three flight phases are distinguished: climb, cruise and descent. For each flight, phases were determined using altitude values sent by aircraft and an indication of aircraft movement (level, climbing or descending) provided by the radar tracker. Top of climb was determined as the point where aircraft leveled and stayed for more than 5 minutes, and either corresponds to the maximum FL, FL_{max}, for this flight, or it is within the range $[FL_{max} - 60, FL_{max}]$. This logic allows to include the stepped cruise phase, when aircraft start their cruise at a lower altitude and then climb to a higher one. A stepped descent in cruise was detected in the same manner as a stepped climb in cruise. Top of descent was determined as the first point where aircraft started descending continuously. Not all flights contained three phases. This did not present difficulties for this study, since for analysis all phases were considered separately from each other.

IV. Parameter Distribution Estimation

In this study, distributions were estimated for the following parameters:

A. Bank angle
B. Speed profile
C. Vertical speed
D. Temporary level-off
E. Atmospheric temperature
F. Wind vector
G. ATC instructions

For parameters from A to E, two types of distributions were obtained: the KDE and the best-fit parametric distribution. The latter was decided upon the results of the Kolmogorov-Smirnov test. Distributions of parameters A to D were obtained per WTC. The determination of parameter F distribution employed a different approach compared to the other parameters and is outlined further in this paper. Distributions of parameters E and F were obtained per season. For parameter G distributions were obtained as an average for the whole year.

A. Bank Angle

There are two data fields sent by aircraft in Mode-S that are relevant for turn detection: roll angle and rate of turn (ROT). Since bank angle data are not available, the roll angle can be assumed to be equal to the bank angle. The difference between the roll angle and the bank angle is zero when the pitch angle is zero and not zero otherwise. The relation between bank ϕ, roll φ, and pitch θ angle is expressed in Eq. (11). Assuming the angle of attack is 0, pitch angle equals the climb/descent angle. Setting, for instance, climb angle to 15 degrees and roll angle to 35 degrees, would result in a bank angle equal to 33.6 degrees, which is 96% of the roll angle.

$$\sin\phi = \sin\varphi\cos\theta \tag{11}$$

Thus, it is reasonable to assume that roll angle equals the bank angle. In this paper, two angles are considered to be same and their names are interchangeable.

Although roll angle data are derived from aircraft, they can be incorrect due to wrong transponder fields' settings. While less than 0.02% of data was erroneous (roll angle values larger than 35 degrees), care must be taken when analyzing these data to filter out unrealistic values. In this study, roll angle values within [5, 35] degrees were considered.

For all sets of records when ROT was within [0.25, 7.5] degrees per second, turn start and end was detected and the maximum roll angle was extracted for each turn. The given range for ROT represents all realistic values for commercial aviation and was estimated using Eq. (12), which shows the relation between ROT, $\dot{\psi}$, roll angle, φ, and true airspeed (TAS) V_{TAS}. In Eq. (12) g is the gravitational acceleration. The minimum ROT was obtained using Eq. (12) for the minimum roll angle of 5 degrees and high cruising TAS equal to 500 knots. The maximum ROT was obtained using

Eq. (12) for the maximum roll angle of 35 degrees and low TAS equal to 100 knots. In ASTERIX Category 062 data, the resolution of ROT is 0.25 degrees per second and obtained maximum and minimum ROT were rounded to 0.25.

$$\dot{\psi} = \frac{g \tan \varphi}{V_{TAS}} \tag{12}$$

In order to capture bank angle settings in a turn, the maximum roll angle was considered. If the average roll angle is used instead, this would include roll-in and roll-out angles, which only show how fast or slow aircraft rolls-in and out of a turn. As a result, small roll angles would reduce the average. When all roll angle values are considered to obtain a distribution, once again roll-in and -out angles would create peaks at smaller roll angles and result in a non-representative distribution. Figure 3 shows an example of a roll angle distribution in the climb phase above FL100 for medium WTC aircraft. When all roll angles are used (Fig. 3a), smaller angles have higher frequency. Average roll reduces the frequency of large angles (Fig. 3b), while distribution based on a maximum roll shows three peaks at 5, 10 and 25 degrees (Fig. 3c).

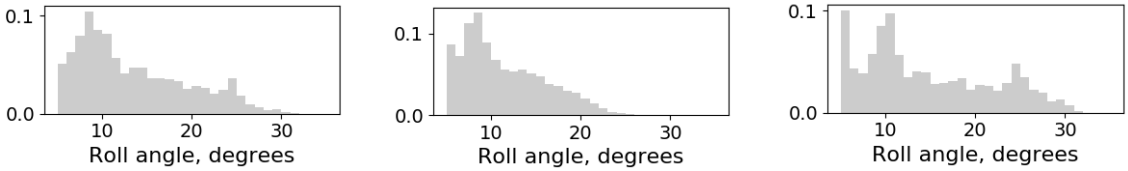

(a) All roll values **(b) Average roll values** **(c) Maximum roll values**

Fig. 3 Roll angle distribution in climb above FL100 for medium WTC. Left: all roll angles, center: average roll angles, right: maximum roll angles.

B. Speed Profile

The speed profile was determined from Mode-S data as a distribution of IAS and Mach number in the climb and descent phases and of Mach number setting in the cruise phase. Usually, speed settings are given in calibrated airspeed (CAS), and IAS is almost identical to CAS only in aircraft clean configuration. In this study, the difference between IAS and CAS is assumed to be not significant.

To ensure a correct extraction of the IAS/Mach profile, *complete* flight phases should be used. In this study, a *complete* climb is from at least FL100 till the top of climb, a *complete* cruise lasts at least 20 minutes, and a *complete* descent is from the top of descent until at least FL100. A complete flight phase is required to detect the crossover altitude. For instance, in the climb phase at a crossover altitude aircraft switch from flying constant CAS to constant Mach. The opposite is true for the descent phase. Table 2 presents the total number of *complete* phases per WTC.

Table 2 Number of complete climb, cruise and descent phases per WTC for 7 days

WTC	Climb	Cruise	Descent
Heavy	3,338	5,340	3,308
Medium	21,021	19,860	19,727
Light	263	361	266
Total	24,622	25,561	23,301

To determine a crossover altitude, segments where IAS and Mach number are constant with time need to be detected and the point where they connect is a crossover altitude. This can be done by looking at the rate of speed change being equal or close to zero.

IAS and Mach number values sent via Mode-S are not the exact pilot/autopilot settings, but measured values. This means that data include some noise, measurement error, and therefore, rarely equal exactly the speed setting. To smoothen the data, a Savitzky-Golay filter was used with a polynomial degree of 3 and window size equal to 61 data points. Then, the 1^{st} and 2^{nd} derivatives were obtained for the smoothed data, which represent the rate of speed change and the rate of the rate of speed change. To reduce the noisy 1^{st} and 2^{nd} derivatives, Savitzky-Golay filters were applied

to both of them with a polynomial degree of 3 and window equal to 7 and 21 data points, respectively. Figure 4 illustrates the approach to constant speed segments' detection in the descent phase. The top plots present the change of IAS (red) and Mach (blue) with flight time. The dashed line is initial data and the solid line is the result of data smoothening. For the 1^{st} derivative (middle plots) and the 2^{nd} derivative (bottom plots) margins (red and blue rectangles) were experimentally determined to capture the segments where the 1^{st} and 2^{nd} derivatives are almost zero. Data points which fall both within, the threshold for the 1^{st} derivative and the threshold for the 2^{nd} derivative, are considered to be the constant speed segment. The detected segments with constant IAS and Mach number are marked in black.

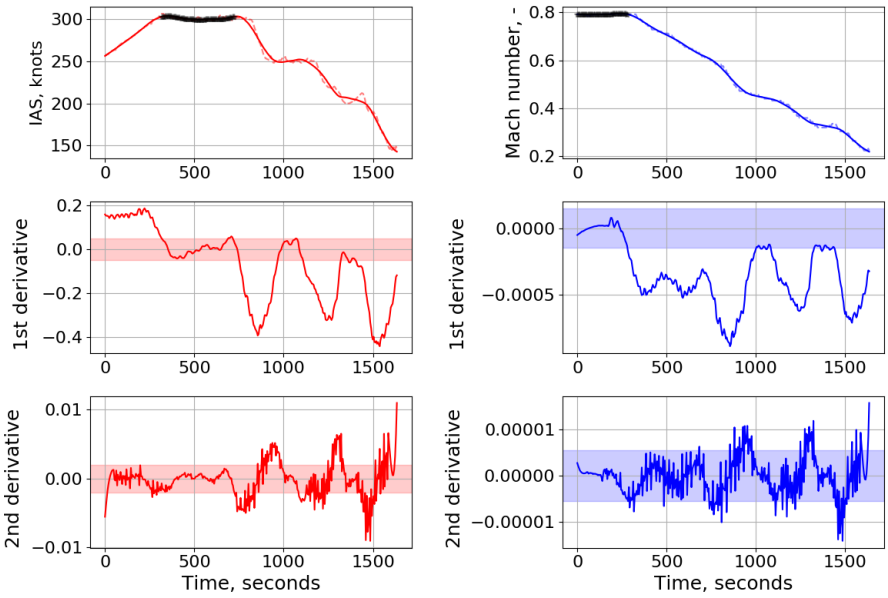

Fig. 4 Constant IAS (red) and constant Mach number (blue) segments detection in the descent phase. Data points that fall within the threshold for the 1^{st} and 2^{nd} derivatives (red and blue rectangles) correspond to constant speed segments. The detected segments of constant speed are marked in black.

C. Vertical Speed

There were two data fields available in the surveillance data with vertical speed indications: barometric vertical rate (BVR) and rate of climb/descent (ROCD). The former is downlinked by aircraft, while the latter is calculated by a ground system. Virtually no differences were identified between the values of these two data fields (difference of 0.03% and 1.6% in the climb and descent phase, respectively), except that ROCD values are one step behind BVR values simply because the ground system computes these values based on the previous observations, while an aircraft transmits its current values. The total difference between the two was determined to be less than 1%. In this study, BVR was used to estimate vertical speed distributions and the term vertical speed is used referring to a barometric vertical rate/speed.

To develop an understanding of how vertical speed is distributed, a two-dimensional histogram of vertical speed versus altitude was plotted. Figure 5 shows an example of a two-dimensional histogram for medium WTC aircraft. The intensity of color represents frequency. In Fig. 5 one can see that the rate of climb (ROC) tends to decrease with an increase in altitude, which is explained by the effect of atmospheric conditions on the engines' performance. There are two regions where ROC drops till about 1,000 feet per minute. These drops occur at around FL30 and just above FL100 and can be explained as follows. At FL30 the noise abatement procedure ends and aircraft can increase power to climb at a higher speed. Above FL100 aircraft are not restricted to 250 knots CAS anymore and can fly at an optimum speed. When accelerating to a higher speed, energy is used on acceleration, which results in less energy available for the climb. In the descent phase, aircraft tend to descend with a fixed vertical speed setting (e.g. 1000, 1500, 2000 feet per minute) until around FL100. Usually, aircraft need to decelerate to comply with the speed restriction of 250 knots CAS below FL100. Additionally, at around this altitude, aircraft start reducing the rate of descent (ROD) for approach. It is obvious that vertical speed depends on altitude due to performance and/or procedures and cannot be correctly described using a single PDF. Therefore, it is reasonable to determine vertical speed distribution as a function of flight phase and altitude.

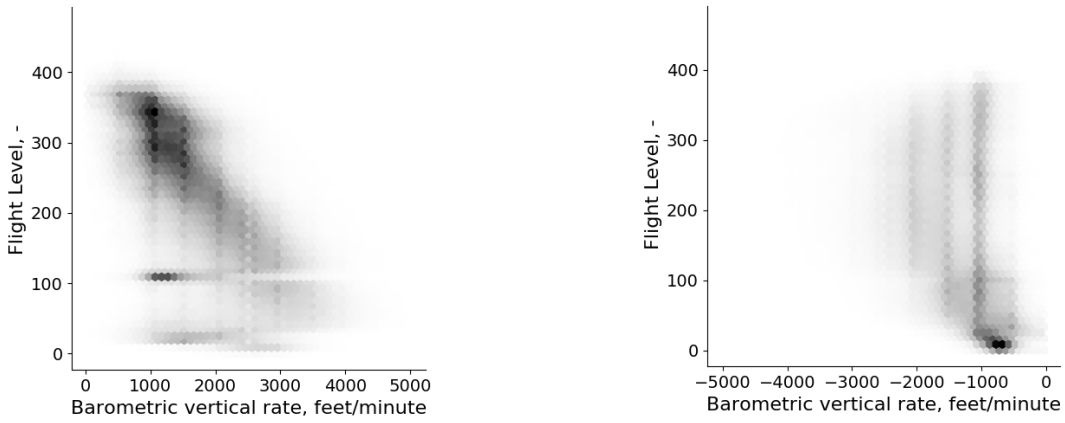

(a) Climb **(b) Descent**

Fig. 5 Two-dimensional histogram of Barometric Vertical Rate versus flight level for medium WTC aircraft in climb (left) and descent (right).

D. Temporary Level-off

A temporary level-off is a leveled flight in the climb or descent phase. Data on temporary level-offs are not readily available and need to be extracted from surveillance data. For this, flights which contain a climb and/or descent phase that lasts for more than 10 minutes were selected. Using the surveillance data flag which indicates the aircraft vertical movement (i.e. climb, level, descent) temporary level-offs in the climb and descent phases were counted and assigned a FL where they occurred together with their duration. Level-offs with duration less than 20 seconds were filtered out, since such short level-offs are most likely a result of an erroneous determination of a level flight by the radar tracker system. However, it is possible that aircraft leveled for such a short period to accelerate/decelerate or aircraft were cleared to continue climb/descent within less than 20 seconds after they have leveled. Level-offs with duration more than 10 minutes comprised 0.12% and 0.3% of level-offs in the climb and descent phases, respectively, and were filtered out. Figure 6 shows a two-dimensional histogram of level-off duration versus flight level in the climb and descent phases for medium WTC. The intensity of color represents frequency. The occurrence of temporary level-offs at particular flight levels and their duration highly depend on the airspace structure, implemented procedures and traffic density.

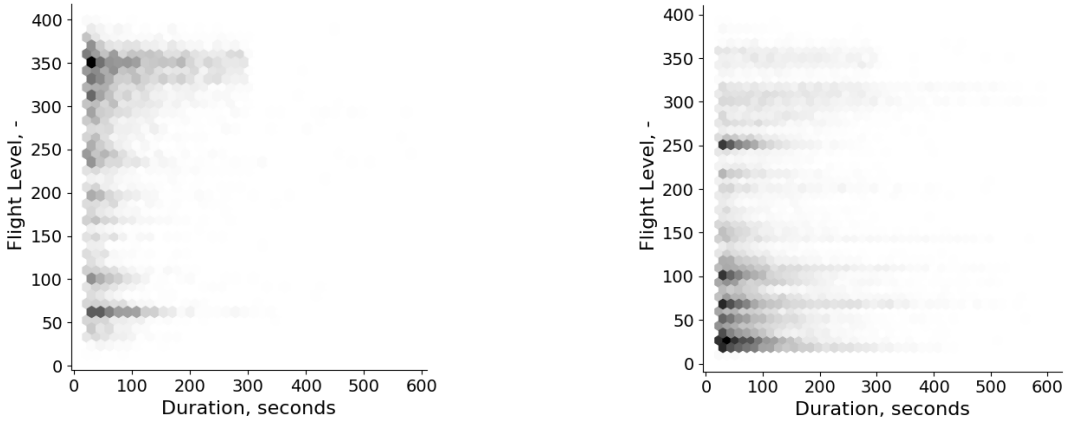

(a) Climb **(b) Descent**

Fig. 6 Two-dimensional histogram of temporary level-offs duration versus flight level for medium WTC aircraft in climb (left) and descent (right).

E. Atmospheric Temperature

Atmospheric temperature changes with seasons and altitude as can be seen in Fig. 7. To describe air temperature, two distributions can be used per season (or month): air temperature distribution at the ground level and lapse rate (i.e. change of air temperature with altitude) distribution.

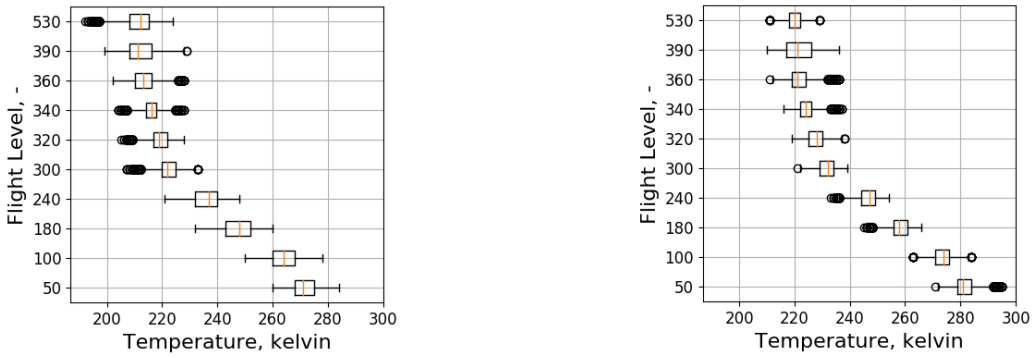

(a) Winter **(b) Summer**

Fig. 7 Box plots of air temperature per flight level for winter (left) and summer (right) forecasts.

The weather forecast used in this study does not provide air temperature values near the ground; the lowest flight level is FL50. Data for this FL were used to determine the distribution of the air temperature near the ground. To allow the computation of the air temperature at altitudes below and above FL50, the lapse rate distribution can be used. This distribution was obtained by taking the average lapse rate below the tropopause for each data point of the forecast. Since the altitude of the tropopause fluctuates, it was determined close to FL360 as the first instance of a constant temperature. Above the tropopause, the air temperature is assumed not to change.

F. Wind Vector

Wind has a stochastic nature and can be defined in terms of speed and direction. A convenient way to display the wind speed and direction together is a wind rose. Figure 8 shows an example of two wind roses (stacked histograms) obtained for all data points at all altitudes for winter and summer. The wind rose shows the frequency and speed of wind blowing from each direction. The circle is divided into 16 spokes, which indicate the wind direction. The concentric circles, which are coming from the center, express the frequency (percentage of time). The length of each spoke indicates the percentage of time the wind is blowing from a particular direction. The colored segments inside each spoke represent the percentage of wind speed ranges.

Whereas the wind speed can be described by a Weibull distribution [43–45], the determination of the wind direction distribution is rather complex since it is represented with angular or circular data. The fact that 0 degrees is the same as 360 degrees and that the mean of 1 and 359 degrees is 0 degrees, and not 180 requires the usage of special techniques for angular data analysis. In some cases, the collected wind data have a prevailing direction, i.e. unimodal, and can be described by the von Mises distribution [46], which is a circular normal distribution. However, when wind data demonstrate several predominant directions, i.e. bimodal or multimodal, an adaptation of present or development of new statistical models is required [46, 47]. Moreover, even when the wind direction can be fit to one of the circular distributions, there is no established way to describe the change of wind direction with altitude (similar to wind gradient).

To overcome all these issues, another way of presenting wind data can be used, which is splitting wind into North-South, denoted v, and West-East, denoted u, components:

$$v = -V_w \cos \psi_w \tag{13}$$

$$u = -V_w \sin \psi_w \tag{14}$$

Here V_w is the wind speed, ψ_w is the wind direction, v is positive in the north direction, and u is positive in the east direction.

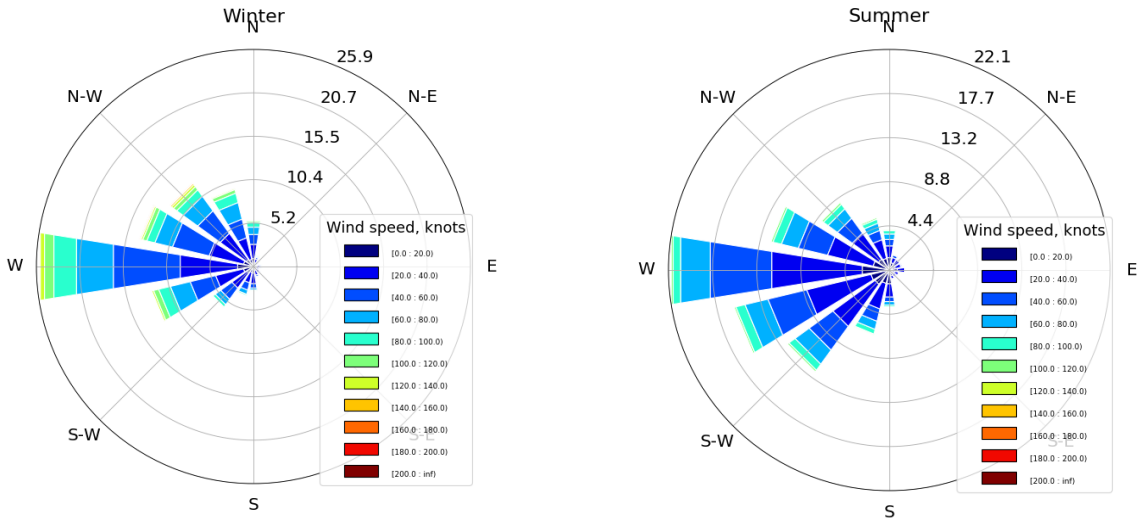

Fig. 8 Wind rose for all data points and altitudes combined for winter (left) and summer (right) forecasts.

Whereas this approach allows to avoid analyzing angular data and to combine wind speed and direction, the variation of wind components with altitude needs to be described. Wind gradient cannot be used, since it describes the change of wind speed only and not applicable to wind components. The estimation of the average rate of wind components with altitude is unsuitable, since positive and negative values cancel each other out and the rate of change is distributed around zero (i.e. wind components do not vary). Therefore, to capture the variability of wind components, the following approach was employed. Firstly, the mean and standard deviation of wind components were estimated for each flight level from data (Fig. 9a). Next, the left and right margins of the data vertical profiles were fitted to a function $f = ax^2 + bx + c$ (Fig. 9b), allowing to estimate the minimum and maximum of a, b and c coefficients. Then, assuming the coefficients are uniformly distributed, these coefficients were randomly sampled allowing the computation of vertical profiles (Fig. 9c). As can be seen in Fig. 9 this approach allows to sample continuous vertical profiles quite accurately. The described example illustrates data for winter forecasts and covers altitudes until FL360. Usually, the tropopause is situated around FL360 and wind components (due to wind speed) exhibit different distributions below and above the tropopause (i.e. wind speed increases with altitude below the tropopause and decreases above the tropopause). To simplify the modeling of the wind components' vertical profile, the values of wind components above the tropopause can be assumed to be equal to those at the tropopause.

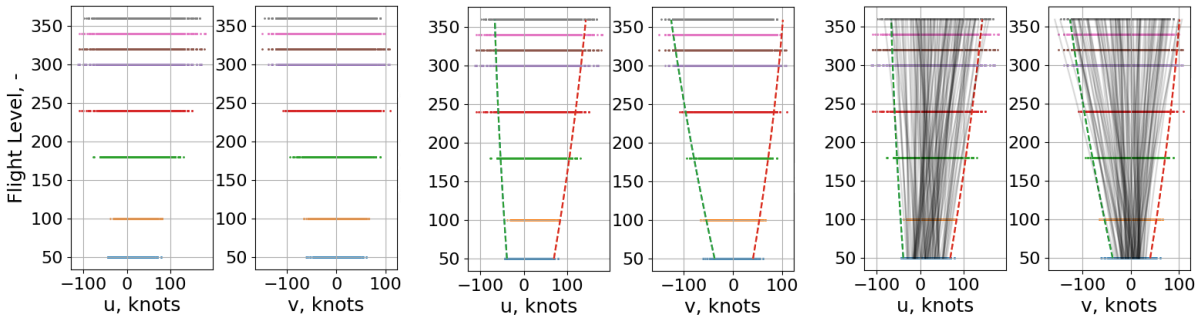

(a) Scatter **(b) Bounds** **(c) Sampling**

Fig. 9 The process of wind components' vertical profile estimation and sampling.

G. ATC Instructions

The frequency of different ATC instructions in a particular airspace largely depends on the type of ATC center (e.g. terminal or en-route). ATCos in a terminal area are likely to give more vertical movement and speed instructions, whereas ATCos in an area control center are likely to give more lateral instructions. In this study, four types of instructions are considered: 'direct', heading, speed and vertical speed. In 2016, on average, 78.6% of flights in MUAC airspace received 1 or more of these instructions (Table 3) and a 'direct' instruction was given to 76.4% of flights (Table 4).

Table 3 Percentage of 1 or more and no ATC instructions

Instructions	%
1 or more	78.6
No instructions	21.4

Table 4 Percentage per instruction type

Instruction type	%
Direct	76.4
Heading	19.1
Speed	6.5
Vertical speed	2.2

Frequencies listed in Table 4 are not meant to add up to 100%, since the same flight can receive all 4 types of instructions. These frequencies show the average amount of flights that received each instruction. While the meaning of such instructions as 'direct', heading and speed is rather clear, the meaning of a vertical speed instruction needs some clarification. An aircraft can be instructed to climb/descend at a specific vertical speed only in combination with the instruction of a cleared flight level. Therefore, statistics on vertical speed instructions were obtained from cleared flight level instructions. Furthermore, the distributions of these four ATC instructions were obtained as PMF since the values of these instructions are discrete (e.g. speed instruction is given as 300 knots IAS and not as 300.53 knots).

V. Results

This section presents the results obtained with the data sets and the methods previously described. Results for such parameters as the bank angle, the speed settings, the vertical speed, the duration of temporary level-offs, the air temperature, the lapse rate and the wind are provided as PDF. The distributions of all parameters except wind are given in both graphical and tabular representations. Graphical representation includes the data distribution histogram, the parametric distribution with the best fit (blue line), the KDE (orange line) and, where applicable, a commonly assumed standard value (red semicircle).

The distributions of the temporary level-offs' flight levels and ATC instructions are given as PMF in both graphical and tabular representations. All graphical representations are provided throughout this section, whereas all tabular representations as well as equations of the distribution functions can be found in the Appendix A and Appendix B respectively. When parameters of a PDF are given in a tabular form, μ is the location, k is the scale and the shape parameters (α, β, c, λ, s) are given according to the distribution definition. When parameters of a uniform distribution are given, these are minimum, a, and maximum, b, values of the distribution.

A. Bank Angle

Figure 10 depicts the roll angle distribution in the climb, cruise and descent phases for heavy, medium and light WTC. The distributions were obtained above FL100 to exclude the high frequency of large roll angles occurring when in holding and when flying standard instrument departure and standard arrival routes. For each WTC, the distributions in the climb and descent phases are similar and have several peaks. These peaks occur at around 5, 10 and 25 degrees and could be a result of the manual selection of (preferred) bank angles or flight management system logic. In the cruise phase, smaller roll angles prevail and peaks occur at around 5 and 10 degrees. This can be explained by small course change angles in the cruise phase. Whereas the distributions for heavy and medium WTC are comparable, the distributions for light WTC are different, which could be a result of a small data set or some performance and/or operational aspects.

On each plot of Fig. 10 the red semicircle indicates a common bank angle setting of 25 degrees. Whereas this value does coincide with one of the peaks in the climb and descent phases, in the cruise phase, 25 degrees bank angle occurs with a low frequency and is not an accurate representation of the bank angle settings. When comparing the KDE and the best-fit distributions, one can see that in some cases the agreement between them is rather good (e.g. climb, cruise

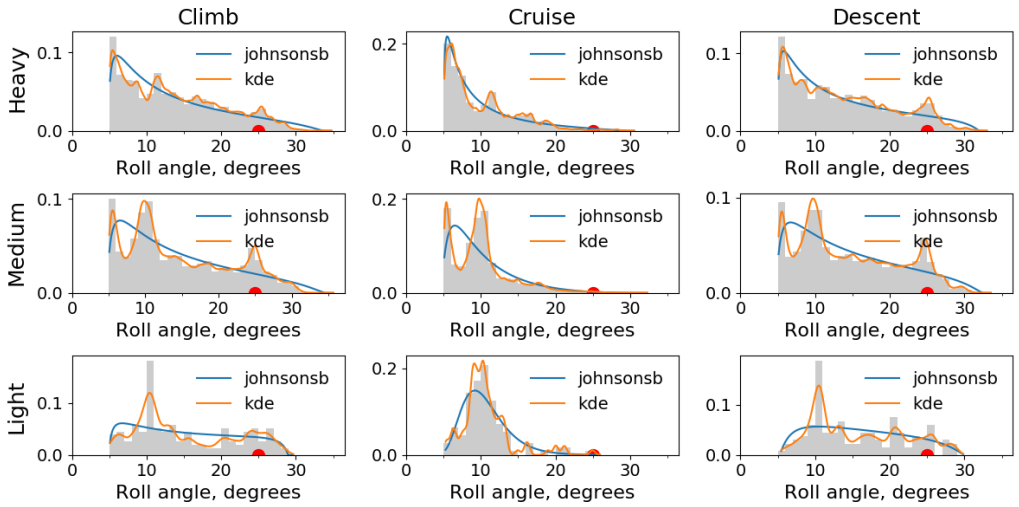

Fig. 10 Roll angle distribution above FL100 in the climb, cruise and descent phases for heavy, medium and light WTC. Red semicircle indicates a commonly assumed bank angle value of 25 degrees.

and descent phase for heavy WTC), whereas in other cases not (e.g. climb and descent phase for light WTC). The types of bank angle distributions and their parameters can be found in Table 8 of the Appendix A.

B. Speed Profile

The described above method to determine aircraft speed profile (see Section IVB) allowed to detect the speed profiles in 60%, 99% and 63% of complete climb, cruise and descent phases (see Table 2), respectively. Such a percentage of detection is due to the fact that aircraft do not always climb/descend at a single constant CAS and Mach number. Often, the climb and descent phases do not include constant CAS or Mach segments or include more than 1. Figure 11 shows examples of speed profiles in the descent phase, which are different from a 'constant Mach constant CAS' descent. In Fig. 11a one could see the absence of a constant Mach segment and a relatively constant IAS segment at the beginning of the descent. In Fig. 11b, after a short constant Mach segment, aircraft decelerates to 250 knots IAS and accelerates to 290 knots. In Fig. 11c there are two constant Mach segments and after switching to IAS at about 1,000 seconds aircraft accelerates to 310 knots IAS.

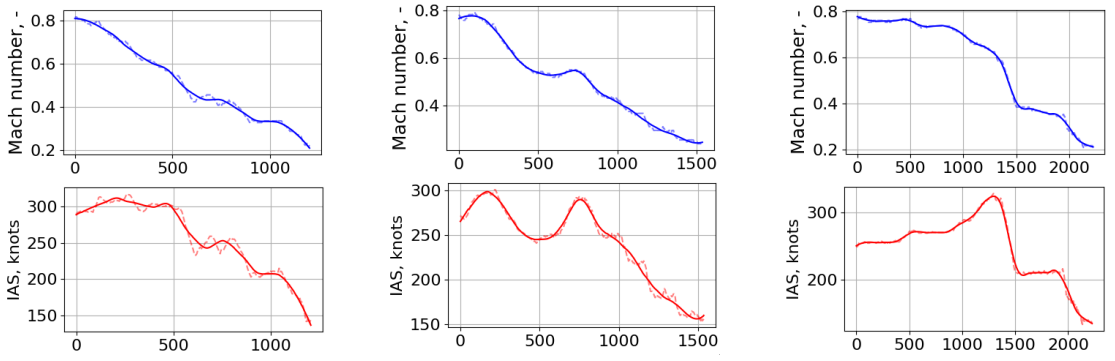

(a) No constant Mach segment **(b) No constant IAS segment** **(c) Two constant Mach segments**

Fig. 11 Speed profile variations in the descent phase.

The data from Airbus and Boeing aircraft types were used to obtain the results for heavy and medium WTC, since these aircraft types comprise 91% and 81% of all aircraft respectively. Figure 12 shows the distributions of IAS and Mach number values in the climb and descent phases and Mach number in the cruise phase for heavy, medium and light WTC. Since speed settings depend on a particular aircraft type, no single commonly assumed value can be provided for

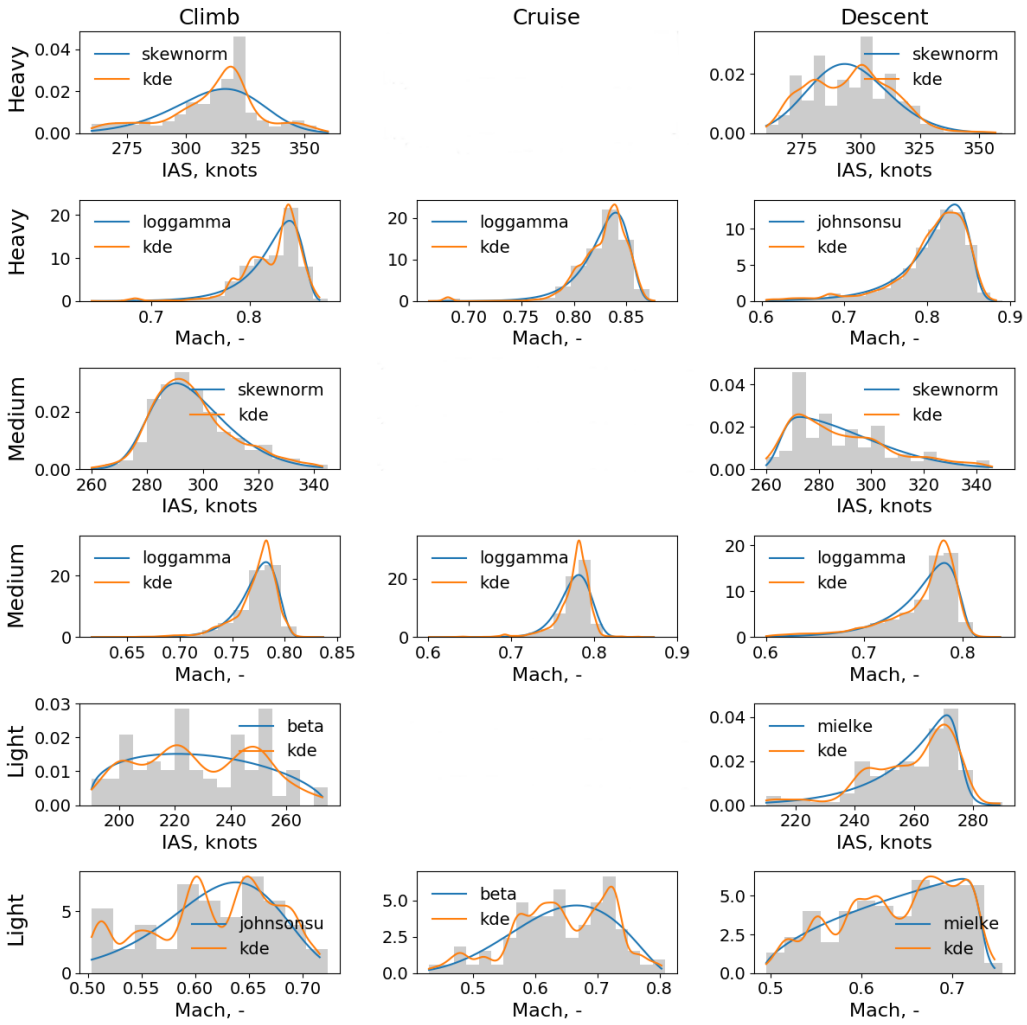

Fig. 12 IAS and Mach number distribution in the climb, cruise and descent phases for heavy, medium and light WTC.

each plot. There is a good agreement between the KDE and the best-fit distributions of Mach number in the climb, cruise and descent phases of all WTCs. The agreement between the KDE and the best-fit distributions is slightly worse for IAS. Although the distributions in Fig. 12 are obtained per WTC and might not be applicable to a particular aircraft type, they do show the variation in speed settings and indicate that an assumption of a single speed value is oversimplified. The types of speed distributions and their parameters can be found in Table 9 of the Appendix A.

C. Vertical Speed

Vertical speed distributions are provided in Fig. 13 for the climb phase and in Fig. 14 for the descent phase. For each WTC, plots like in Fig. 5 were used to determine the altitude ranges, which demonstrated similar distributions of the vertical speed. These altitude ranges are provided in FLs at the top of each plot. For instance, *FL0-FL40* indicates that the distribution was obtained for the vertical speed between FL0 and FL40. Altitude ranges of the form *FL300-max* and *FL0-max* indicate that the distribution was obtained for the vertical speed above FL300 and above FL0 respectively. Plots with altitude range *FL0-max* are given to show the combined vertical speed distribution over all altitudes.

The distributions for heavy and medium WTC are very similar and were obtained for the same altitude ranges. Light WTC has somewhat different altitude ranges for the vertical speed distributions, which can be explained by the speed settings. Often, light aircraft do not climb/descend faster than 250 knots CAS above FL100. This results in fewer

aircraft accelerating/decelerating after/prior to FL100 and as a consequence fewer aircraft reducing their vertical speed. The reduction of vertical speed can be observed in plots with altitude ranges FL105-FL120 for heavy and medium WTC. These plots show that the majority of aircraft trade off vertical speed for CAS acceleration. A long flat tail on the right of the distributions indicates that some aircraft either do not lose much energy on acceleration or accelerate fast/slow to the preferred climbing CAS. Almost all plots for heavy and medium WTC demonstrate a good agreement between the KDE and the best-fit parametric distributions. Exceptions are altitude ranges FL40-FL105 and FL105-FL120 in climb and FL110-max in descent. The distributions in these ranges are bimodal and indicate that the substantial amount of aircraft climb/descend slower/faster than the majority. For light WTC the best-fit distributions do not agree well with the KDE due to bi- or multimodality of the data distributions. Multiple peaks in distributions could be a result of too little data available for light WTC. The types of vertical speed distributions and their parameters can be found in Tables 10, 11, 12, 13 of the Appendix A.

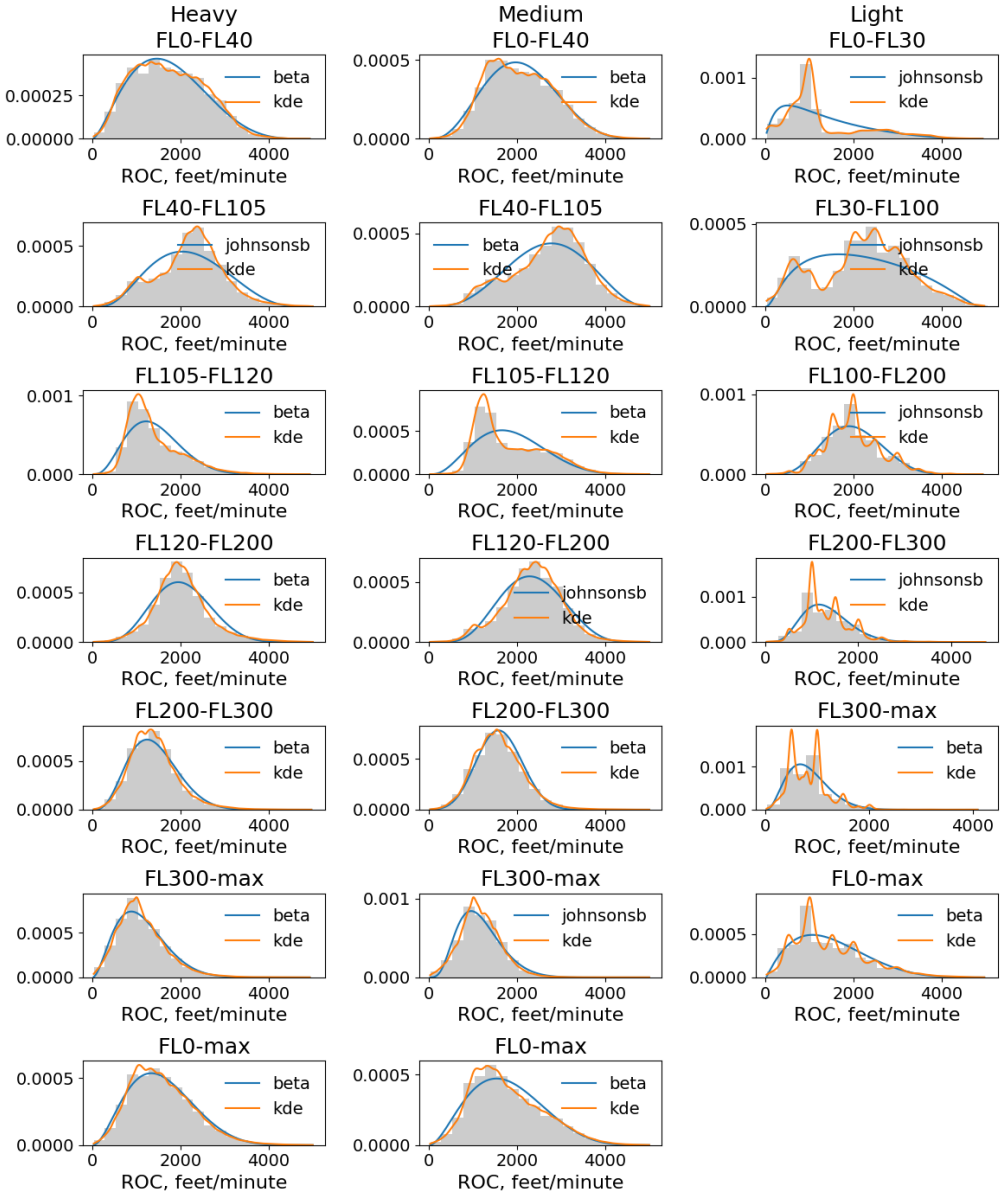

Fig. 13 Vertical speed distribution in the climb phase per FL ranges for heavy, medium and light WTC.

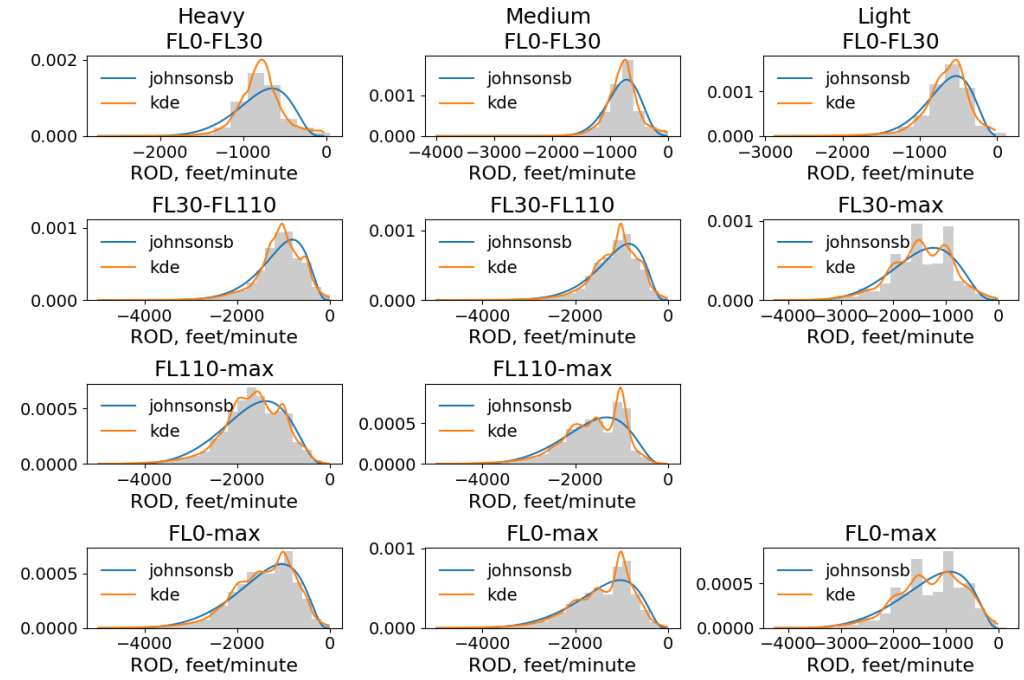

Fig. 14 Vertical speed distribution in the descent phase per FL ranges for heavy, medium and light WTC.

D. Temporary Level-off

Figure 15 shows the distributions of the FLs where temporary level-offs occur and their duration for heavy, medium and light WTC above FL100 in the climb and descent phases. These distributions are very dependent on the airspace (configuration), implemented procedure and ATC. For instance, in the climb and descent phases, there are peaks at FL240 and FL260 respectively, which are due to aircraft transfer to and from MUAC airspace. Similarly, other temporary level-offs occur as a result of internal procedures to transfer aircraft from a sector to a sector, aircraft waiting for ATC clearances and ATC conflict resolutions.

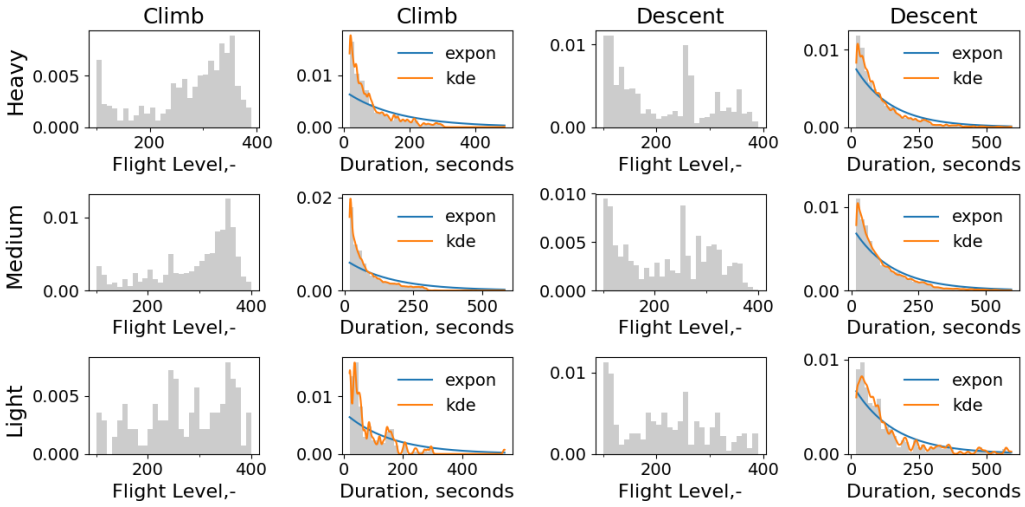

Fig. 15 Distribution of the flight levels and duration of the temporary level-offs above FL100 in the climb and descent phases for heavy, medium and light WTC.

The exponential distribution was determined to be the best-fit distribution for temporary level-offs duration. Data

shows that level-offs may last up to 10 minutes, however, the majority of temporary level-offs last less than 100 seconds. Longer temporary level-offs (more than 5-7 minutes) might be actually a part of climbs/descents in cruise and might have been included in the distributions as a result of how flight phases were determined when pre-processing data (see Section 2). In the descent phase, the exponential distribution agrees well with KDE, whereas in the climb phase the exponential distribution does not fit the peaks at short durations. The distributions of temporary level-offs' FLs are represented with PMFs; therefore, no fitted distributions are given. The distributions of temporary level-offs' duration and their parameters can be found in Table 14 of the Appendix A, whereas the PMFs of temporary level-offs' FLs are in Tables 15 and 16 of the Appendix A.

E. Air Temperature

To describe the variation of air temperature, the distributions of two parameters were obtained: the air temperature near the ground and the lapse rate. Figure 16 shows the distributions of the air temperature near the ground (FL50) per season and for the whole year. Red semicircles indicate the air temperature at FL50 according to ICAO ISA. Whereas this ISA temperature value is close to the mean values of the autumn and whole year distributions, it is rather far from the mean values for the rest of the distributions. Also, all air temperature distributions are bimodal, indicating that the choice of grouping data by seasons might not be the most suitable one. Instead, the data could be grouped by months. By taking the difference between the air temperature distributions and ISA temperature, these distributions could be converted into the distributions of the temperature offset from ISA. There is a good agreement between the best-fit distributions and the KDE in Fig. 16. The air temperature distributions and their parameters can be found in Table 17 of the Appendix A.

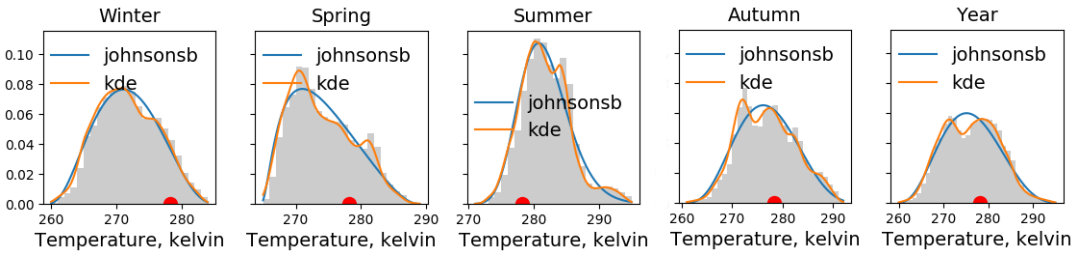

Fig. 16 Air temperature distribution near the ground (FL50) per season and for the whole year. Red semicircle indicates the standard temperature (i.e. according to ICAO ISA).

Figure 17 shows the distributions of the lapse rate below the tropopause per season and for the whole year. Red semicircles indicate the standard lapse rate according to ICAO ISA which is -6.5 kelvin per kilometer. All lapse rate distributions are very similar; the shape of the distributions varies, whereas the minimum and maximum values are almost the same. For all distributions, the standard lapse rate is a good approximation of the mean value. Nonetheless, the variation of the lapse rate is significant. There is a good agreement between the best-fit distributions and the KDE in Fig. 17. The lapse rate distributions and their parameters can be found in Table 17 of the Appendix A.

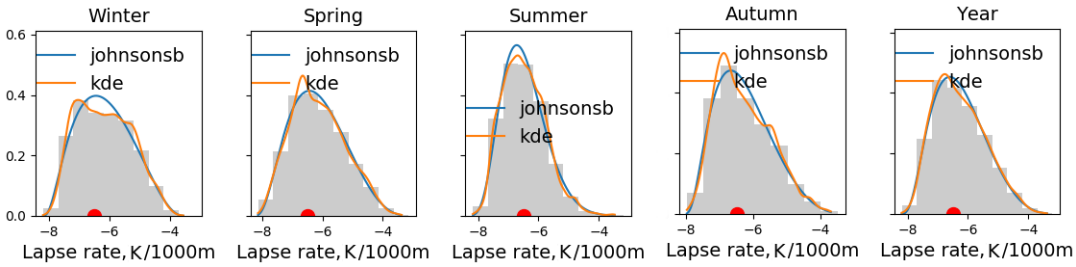

Fig. 17 Lapse rate distribution below the tropopause per season and for the whole year. Red semicircle indicates the standard lapse rate (i.e. according to ICAO ISA).

F. Wind Vector

Following the approach outlined in Section F, the coefficients (a, b, c) of the function that approximates the vertical profile of u and v wind components were estimated and are provided in Table 18 of the Appendix A. The uniform distribution is used to define the coefficients since it resulted in the best coincidence between the wind speed and direction distributions obtained from the input data (i.e. weather forecasts), and the data obtained from the wind components' vertical profile approximation.

G. ATC Instructions

The distributions of four ATC instructions' types, namely 'direct', heading, speed and vertical speed, were estimated. These distributions are very specific to the internal procedures and practices of the considered airspace. Since MUAC ATC data were used in this study, the obtained results might not be applicable to other ATC centers. Moreover, when interpreting the results for each instruction type outlined below, the frequency of flights that received an instruction should not be confused with the total number of flights. For instance, a heading instruction is given, on average, to 19.1% of flights. Out of this 19.1%, 86% of flights receive an instruction to stay on the present heading, which is 16.4% of all flights.

There are two types of 'direct' instructions that can be given: direct-to and direct-via. Direct-to is given 80% of the time (Fig. 18). There are four types of heading instructions: present heading, heading (value), turn left and turn right. Figure 19 shows that 86% of the flights receive a present heading instruction. The small number of turn right and turn left instructions, instructions that are commonly given to resolve conflicts, is rather surprising. Actually, the majority of turn left and turn right instructions were input to a system as a present heading instruction due to some system input interface aspects. As a result, the large number of present heading instructions and the small number of turn right and turn left instructions do not correctly represent real statistics. The PMFs of 'direct' and heading instructions can be found in Tables 19 and 20 of the Appendix A.

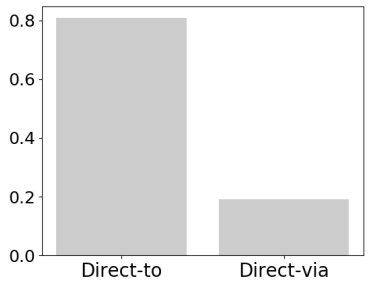

Fig. 18 Distribution of 'direct' instructions.

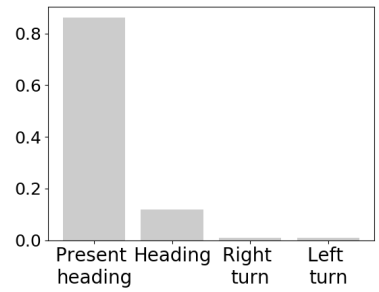

Fig. 19 Distribution of heading instructions.

There are four types of speed instructions: assigned, maximum, minimum and present speed (Fig. 20). An instruction to fly at the assigned speed is given to almost 50% of flights, whereas an instruction to keep the present speed is almost never given. Two types of speeds can be given with a speed instruction: Mach number or IAS. Mach number is given nearly 70% of the time (Fig. 21). The high percentage of speed instructions given as a Mach number makes sense as the upper airspace encompasses the en-route part of the flights, where aircraft fly at the constant Mach number. The PMFs of Mach number and IAS values given by ATC as a speed instruction are presented in Fig. 22 and Fig. 23, respectively. All PMFs related to the speed instructions can be found in Tables 21, 22, 23 and 24 of the Appendix A.

A vertical speed (VS) instruction can be an instruction to climb (ROC) or to descend (ROD). ROD is given in slightly over 80% of the cases (Fig. 24). Together with the VS type, an instruction can include an indication of the speed limit: minimum or maximum. If such a limit is given, almost always, it is a minimum value (Fig. 25). The PMFs of ROD and ROC are presented in Fig. 26 and Fig. 27, respectively. As can be seen ATC rarely instructs aircraft to climb or descend at large vertical speeds. The most frequent values are 1,000 feet per minute in climb and -1,500 feet per minute in descent. All PMFs related to VS instructions can be found in Tables 25, 26, 27 and 28 of the Appendix A.

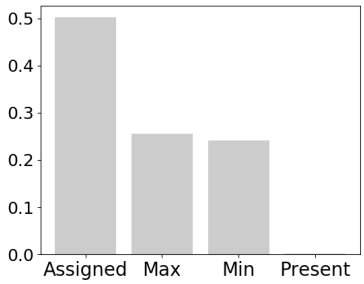

Fig. 20 Distribution of speed instruction types.

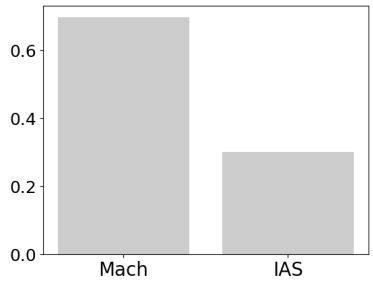

Fig. 21 Distribution of speed types.

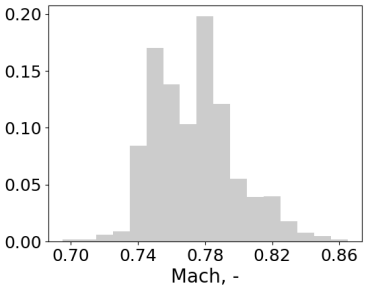

Fig. 22 Distribution of Mach speed instructions.

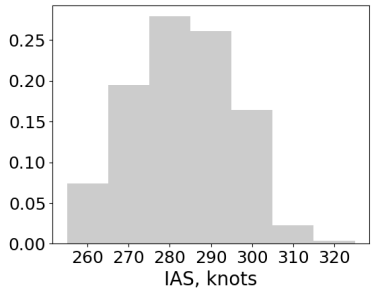

Fig. 23 Distribution of IAS speed instructions.

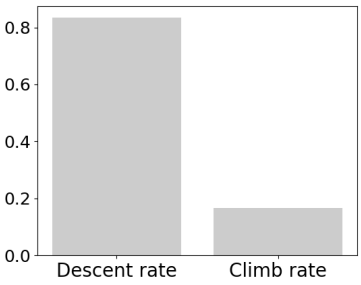

Fig. 24 Distribution of VS instruction types.

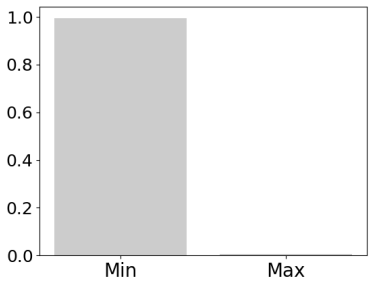

Fig. 25 Distribution of VS instruction limits.

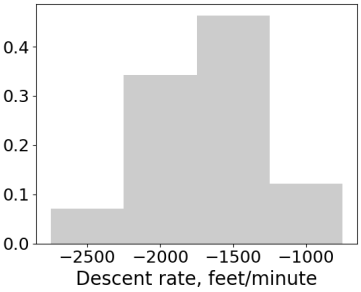

Fig. 26 Distribution of ROD instructions.

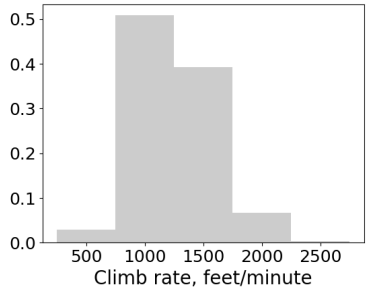

Fig. 27 Distribution of ROC instructions.

VI. Discussion

This section reviews some common assumptions about bank angle, speed profile and temporary level-offs in the climb and descent phases. Additionally, a potential benefit from using parameter distributions instead of single parameter settings is addressed. Finally, the impact of ATC instructions on the studied parameters and the relevance of the results from this paper are discussed.

A. Bank Angle

When interpreting the bank angle distributions as a function of a flight phase, it is useful to look at the course change angles in each phase. Figure 28 shows the frequency of course change angle values, where on the x-axis each angle indicates the values less than the given value. For instance, the bars at 10 degrees course change angle represent angles from 1 to 10 degrees. In the cruise phase, about 67% of turns are not larger than 10 degrees, which explains the high frequency of small bank angles. In general, turns larger than 50 degrees almost do not occur in cruise. In addition, in both climb and descent phases, turns smaller than 10 degrees comprise nearly 50% of all turns. For a large turn angle (i.e. 40 degrees and more), a bank angle of 20 degrees or more is required to complete the turn fast. This explains peaks at 25 degrees in the bank angle distributions for climb and descent phases. Nevertheless, an assumption of a single bank angle setting of 25 or 35 degrees is inaccurate.

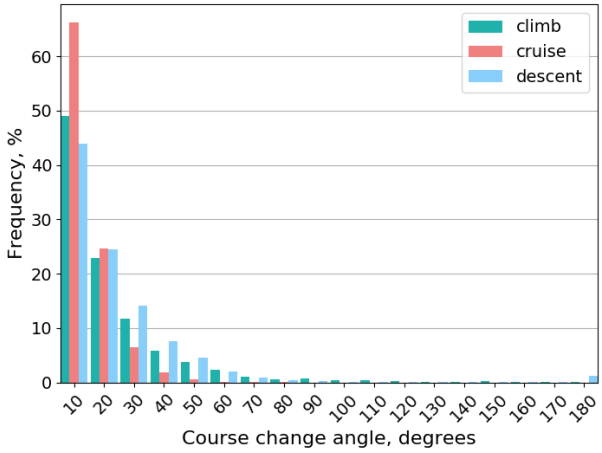

Fig. 28 Magnitude and frequency of course change angles per flight phase.

B. Speed Profile

It is a common assumption that aircraft climb and descend at a 'constant CAS constant Mach' speed profile. In reality, this is not always the case and other variations of speed profiles also occur. This makes it difficult to estimate aircraft speed settings from observed data. Another prevalent assumption, which is more a rule, is that aircraft fly at a speed of 250 knots CAS/IAS below FL100. The origin of this is in the speed restrictions defined by ICAO for several airspace classes, operational aspects of terminal areas (e.g. sequencing and merging) and the risk of bird strikes. Aircraft can fly faster only if instructed by ATC. Table 5 shows the average percentage of flights that flew faster than 250 knots IAS below FL100. The percentage is low for light WTC since, in general, light aircraft do not climb/descend faster than 250 knots IAS. Heavy and medium aircraft, however, do prefer climbing/descending faster than 250 knots. A rather high percentage for these WTCs could be a result of ATC instructing aircraft to fly faster when the traffic situation permits or for sequencing/merging purposes. Furthermore, no correlation was found between these flights and the time of a day or geographic location.

C. Temporary Level-off

Temporary level-offs are often disregarded when performing trajectory prediction studies. Operational trajectory predictors will include temporary level-offs if they are indicated in the flight plan. In most cases, temporary level-offs occur as a result of ATC procedures, separation or due to delays on the ground. Table 6 shows the average percentage

Table 5 Average percentage of flights not restricted to 250 knots IAS below FL100 per WTC for 7 days

WTC	Climb, %	Descent, %
Heavy	29.04	24.64
Medium	10.77	28.97
Light	2.84	9.07

of flights that temporarily level-off in the climb and descent phases. The percentage is strikingly high for all WTCs and almost twice more flights experience temporary level-offs in the descent compared to the climb phase. Moreover, one flight can encounter up to 5 temporary level-offs in climb and up to 7 level-offs in descent. Although temporary level-offs can occur unpredictably, the high frequency of their occurrence indicates the necessity to include them in the prediction process.

Table 6 Average percentage of flights with temporary level-offs per WTC for 7 days

WTC	Climb, %	Descent, %
Heavy	32.05	66.62
Medium	32.93	61.41
Light	44.49	73.27

D. Single Parameter Setting versus Parameter Distribution

Often, when performing trajectory prediction studies or obtaining predictions from operational trajectory predictors, trajectory predictor inputs are assumed to be fixed to a certain value, which results in a single trajectory prediction. In reality, this is obviously not the case, and the majority of parameters dynamically change based on many aspects (e.g. procedures, performance, policies), some of which may be unknown (in advance). In an attempt to cope with this uncertainty, trajectories could be predicted in a probabilistic way, where several trajectories are predicted for a single flight based on the inputs' PDFs. This approach would result in ensemble prediction, similar to ensemble weather forecasting. Each prediction would have its probability of occurring where the probability could be estimated as a proportion of the ensemble members (i.e. predictions) that predicted certain events (e.g. time at waypoint).

Clearly, not all decision support tools could use and benefit from probabilistic predictions. Applications that operate for short look-ahead times and where predictions are updated using real-time surveillance data (e.g. short term conflict detection) have much less uncertainty. For these applications, it might be not worthwhile to consider multiple predictions for a single flight. However, decision support tools that look at longer look-ahead times and do not have the luxury of real-time updates with surveillance data (e.g. MTCD and traffic flow management tools), could potentially gain from using ensemble prediction. This, of course, would require to adapt these tools to take probabilistic predictions as input. Furthermore, probabilistic predictions could be used for research purposes and in air traffic management related studies.

E. Impact of ATC on Aircraft Parameters

ATC can instruct aircraft to fly a certain heading, IAS/Mach number or vertical speed. These instructions are issued for separation/sequencing purposes and pilots will comply if possible. Thus, observed aircraft parameters, such as the bank angle in turns, the speed settings and the vertical speed, are partly influenced by ATC and might not be related to aircraft performance. The extent of this influence is, of course, proportionate to the frequency of instructions.

F. Results Relevance

Some results of this study are valid for the geographic region outlined in Section III and might be not representative for other geographic regions. Such parameters as air temperature, lapse rate and wind are very dependent on the geographic location, and the distributions obtained for these parameters must be treated with caution. Same holds for the ATC instructions, which were obtained for MUAC airspace. Furthermore, some of the obtained distributions (e.g. speed settings) depend on the methods employed for their estimation and might be different if other methods are used.

VII. Conclusion

In order to improve the accuracy of trajectory predictions, the quality of the input data, whose exact values are often unknown, must be improved. Whereas it is convenient to use fixed values for the trajectory predictor inputs, such a simplified assumption is far from reality.

This paper demonstrated the variability of the trajectory predictor inputs by deriving their distributions from observed data. The studied parameters are bank angle, speed settings, vertical speed, temporary level-offs, air temperature, lapse rate, wind vector and ATC intent. To generalize results, where applicable, the distributions were obtained per WTC. In many cases, the results for heavy and medium WTC were similar, whereas the results for light WTC were often significantly different from heavy and medium WTC. For the atmospheric conditions and weather-related parameters, the distributions were derived per season. The distributions were obtained as PDF or PMF depending on the type of variables (i.e. continuous or discrete). For each PDF, two types of distributions were estimated: a best-fit parametric distribution and a non-parametric KDE, which is the most accurate representation of data distribution. In many cases, there was a good agreement between them. The distributions were provided in both graphical and tabular form, which allows to reproduce the parametric distributions. Although the ATC intent is highly dependent on the airspace type and internal procedures and practices, this paper provided with indicative results on the frequency of the main ATC instructions. This paper also addressed some common assumptions about the specific fixed values of several parameters.

Future research could be conducted to investigate the potential benefits from using the inputs' PDFs instead of single values. Ensemble prediction, a concept similar to ensemble weather forecasting, could allow to improve the performance of the decision support tools that operate at medium look-ahead time (e.g. MTCD).

Acknowledgments

The authors would like to thank Kristof Schippers, Marcin Piatek, Zoltan Peczoli, Torsten Doernbach from MUAC, EUROCONTROL, for providing insights into ATC inputs and surveillance data.

Appendix A

Table 7 Summary on parameters' settings from previous research

Reference	Parameter	Note
	Bank angle. Take-off (TO), landing (LND)	
Mondoloni [5]	maximum 25 degrees	
BADA [12]	nominal 15 /35 degrees	TO, LND /other phases
	maximum 25 /45 degrees	TO, LND /other phases
Glover [14]	nominal 35 degrees	
Camilleri [15]	*constant*	
Lee [16]	*default*	
	Speed. Climb/Cruise/Descent (CL/CR/DES). Knots IAS (KIAS), knots CAS (KCAS)	
Mondoloni [8]	reference CAS/Mach $\pm 5, 10\%$	
BADA [12]	CL/CR/DES CAS/Mach	per aircraft type
Sun [17]	CL/CR/DES CAS/Mach	per aircraft type
Slater [18]	DES 340KCAS ± 15, Mach $\in$ [0.8, 0.84]	Boeing-767
Torres [19]	DES KCAS $\in$ [265, 320]	Boeing-737-700
McConkey [20]	DES slow-speed (0.76/240KIAS)	Boeing-737-100
	DES medium-speed (0.73/280KIAS)	Boeing-737-100
	DES high-speed (0.76/320KIAS)	Boeing-737-100
Alligier [21]	reference CAS + $\boldsymbol{U}$ (-30, 30)	
	reference Mach + $\boldsymbol{U}$ (-0.03, 0.03)	
Casado [23]	DES CAS $\boldsymbol{Tri}$ (298.2, 7.8, NA)	Boeing-747-400
	Vertical speed	
Sun [17]	vertical speed	per aircraft type
Suchkov [24]	climb/descent rate $\in$ [600, 4000] feet per minute	
Jones [25]	descent rate $\in$ [200, 6500] feet per minute	Boeing-747-400
	Temporary level-off	
Mondoloni [4] [5]	occurrence 28%, duration 5-60 minutes, altitudes FL110-350, peak FL310	in climb
Mondoloni [8]	occurrence 27%	of total flights
	duration 1-4 minutes	
	length 5, 10, 15, 20 nautical miles	
Eurocontrol [26]	occurrence in climb 19%, peaks in climb FL60, FL320-340	of total flights
	occurrence in descent 42%, peaks in descent FL30, FL300	of total flights
	duration 1-20 minutes	
	altitudes FL20-440	
Roach [27]	occurrence in descent 20%, average duration 1.67 minutes	of all departures
Miller [28]	climb:	
	occurrence 27%, mean duration 2.88 minutes	regional level
	occurrence 14.3%, mean duration 2.82 minutes	national level
	peak in climb FL160	
	descent:	
	occurrence 64.5%, mean duration 3.92 minutes	regional level
	occurrence 59.6%, mean duration 3.52 minutes	national level
	peaks in descent FL100, FL230	
	Weather forecast (Air temperature, wind vector)	
Mondoloni [8]	wind bias $\pm 10, 20$ knots	
	wind gradient $\pm 1.5, 3$ knots/1000feet	
Alligier [21]	temperature offset ΔT $\boldsymbol{U}$ (-20, 20)	
ICAO [29]	standard atmospheric conditions	
Smith [30]	variations of the temperature profile	
Gallo [33]	wind speed linear decrease from 150 knots at FL360 to 0 knots at sea level	
Hernandez [34]	uniform distribution, mean varies between -20 and 20 meters per second	speed components
	half-width varies between 0 and 25 meters per second	
Kim [35]	mean wind of 30.5 knots (35 miles per hour)	
	standard deviation of 17 knots (20 miles per hour)	
Robert [36]	wind speed from 0 knots to 160 knots	over Europe
	wind average of 32 knots	
	wind direction North-West (220-310 degrees)	

Table 8 PDF of bank angle in climb, cruise and descent for heavy, medium and light WTC

WTC	Climb
Heavy	Johnson SB (α=0.82, β=0.70, μ=4.78, k=29.03)
Medium	Johnson SB (α=0.71, β=0.71, μ=4.71, k=29.93)
Light	Johnson SB (α=0.24, β=0.63, μ=4.93, k=24.07)
WTC	Cruise
Heavy	Johnson SB (α=1.32, β=0.70, μ=4.99, k=24.90)
Medium	Johnson SB (α=1.65, β=0.99, μ=4.46, k=27.96)
Light	Johnson SB (α=13.45, β=2.81, μ=2.06, k=973.06)
WTC	Descent
Heavy	Johnson SB (α=0.70, β=0.64, μ=4.91, k=27.13)
Medium	Johnson SB (α=0.61, β=0.71, μ=4.71, k=27.82)
Light	Johnson SB (α=0.29, β=0.78, μ=5.13, k=25.07)

Table 9 PDF of speed settings in climb, cruise and descent for heavy, medium and light WTC

WTC	Speed	Climb
Heavy	IAS	Skew-normal (α=−1.98, μ=331.38, k=28.00)
	Mach	Log-Gamma (c=0.43, μ=0.85, k=0.01)
Medium	IAS	Skew-normal (α=3.03, μ=280.02, k=22.05)
	Mach	Log-Gamma (c=0.84, μ=0.78, k=0.01)
Light	IAS	Beta (α=1.35, β=1.61, μ=189.45, k=85.10)
	Mach	Johnson SU (α=11.30, β=3.85, μ=0.84, k=0.02)
WTC	Speed	Cruise
Heavy	Mach	Log-Gamma (c=0.69, μ=0.84, k=0.01)
Medium	Mach	Log-Gamma (c=2.50, μ=0.75, k=0.03)
Light	Mach	Beta (α=4.82, β=2.73, μ=0.33, k=0.49)
WTC	Speed	Descent
Heavy	IAS	Skew-normal (α=1.31, μ=281.10, k=22.51)
	Mach	Johnson SU (α=2.54, β=1.57, μ=0.87, k=0.02)
Medium	IAS	Skew-normal (α=9.14, μ=264.93, k=31.10)
	Mach	Log-Gamma (c=0.33, μ=0.79, k=0.01)
Light	IAS	Mielke's Beta-Kappa (λ=15.63, s=155.36, μ=−1.87, k=277.15)
	Mach	Mielke's Beta-Kappa (λ=1.56, s=49.40, μ=0.49, k=0.24)

Table 10 PDF of vertical speed in climb per FL ranges for heavy and medium WTC

WTC	FL0-40
Heavy	Beta (α=2.58, β=4.74, μ=3.25, k=4893.75)
Medium	Beta (α=3.83, β=5.38, μ=20.88, k=4962.50)
WTC	FL40-105
Heavy	Johnson SB (α=0.37, β=1.37, μ=8.38, k=4962.50)
Medium	Beta (α=4.12, β=3.54, μ=43.48, k=4962.50)
WTC	FL105-120
Heavy	Beta (α=3.73, β=9.52, μ=29.00, k=4893.75)
Medium	Beta (α=3.34, β=5.94, μ=61.58, k=4962.50)
WTC	FL120-200
Heavy	Beta (α=5.63, β=8.34, μ=27.46, k=4962.50)
Medium	Johnson SB (α=0.27, β=1.68, μ=43.02, k=4962.50)
WTC	FL200-300
Heavy	Beta (α=4.40, β=11.19, μ=6.50, k=4931.25)
Medium	Beta (α=10.49, β=13.33, μ=-579.60, k=4962.50)
WTC	FL300-max
Heavy	Beta (α=2.98, β=10.02, μ=0.77, k=4893.75)
Medium	Johnson SB (α=2.10, β=1.85, μ=-99.78, k=4962.50)
WTC	FL0-max
Heavy	Beta (α=2.98, β=6.43, μ=10.90, k=4962.50)
Medium	Beta (α=2.81, β=5.11, μ=17.85, k=4962.50)

Table 11 PDF of vertical speed in climb per FL ranges for light WTC

WTC	FL0-30
Light	Johnson SB (α=1.12, β=0.94, μ=-43.19, k=4893.75)
WTC	FL30-100
Light	Johnson SB (α=0.28, β=0.93, μ=-1.61, k=4931.25)
WTC	FL100-200
Light	Johnson SB (α=0.56, β=1.79, μ=-101.49, k=4893.75)
WTC	FL200-300
Light	Johnson SB (α=1.76, β=1.96, μ=-91.63, k=4706.25)
WTC	FL300-max
Light	Beta (α=3.43, β=13.45, μ=15.16, k=4062.50)
WTC	FL0-max
Light	Beta (α=2.07, β=4.95, μ=17.71, k=4931.25)

Table 12 PDF of vertical speed in descent per FL ranges for heavy and medium WTC

WTC	FL0-30
Heavy	Johnson SB (α=−1.57, β=1.64, μ=−2718.94, k=2718.75)
Medium	Johnson SB (α=−2.62, β=2.69, μ=−3651.69, k=3968.75)
WTC	FL30-110
Heavy	Johnson SB (α=−2.12, β=1.60, μ=−4926.19, k=4962.50)
Medium	Johnson SB (α=−2.03, β=1.55, μ=−4962.74, k=4962.50)
WTC	FL110-max
Heavy	Johnson SB (α=−1.11, β=1.48, μ=−4972.59, k=4962.50)
Medium	Johnson SB (α=−1.17, β=1.45, μ=−4981.95, k=4962.50)
WTC	FL0-max
Heavy	Johnson SB (α=−1.33, β=1.33, μ=−4964.29, k=4962.50)
Medium	Johnson SB (α=−1.38, β=1.35, μ=−4965.89, k=4962.50)

Table 13 PDF of vertical speed in descent per FL ranges for light WTC

WTC	FL0-30
Light	Johnson SB (α=−1.87, β=1.77, μ=−2737.65, k=2850.00)
WTC	FL30-max
Light	Johnson SB (α=−1.02, β=1.52, μ=−4199.27, k=4225.00)
WTC	FL0-max
Light	Johnson SB (α=−1.15, β=1.29, μ=−4196.63, k=4225.00)

Table 14 PDF of temporary level-offs duration in climb and descent for heavy, medium and light WTC

WTC	Climb	Descent
Heavy	Exponential (μ=17.99, k=158.35)	Exponential (μ=18.99, k=133.95)
Medium	Exponential (μ=17.99, k=166.48)	Exponential (μ=17.99, k=146.52)
Light	Exponential (μ=18.99, k=156.47)	Exponential (μ=18.99, k=150.33)

Table 15 PMF of temporary level-off FLs in climb for heavy, medium and light WTC

WTC\FL	100	110	120	130	140	150	160	170	180	190	200	210	220	230	240	250
Heavy	0.065	0.022	0.021	0.018	0.006	0.018	0.007	0.011	0.021	0.013	0.019	0.006	0.013	0.017	0.043	0.038
Medium	0.033	0.021	0.008	0.011	0.005	0.020	0.006	0.023	0.012	0.016	0.028	0.015	0.010	0.021	0.050	0.024
Light	0.036	0.029	0.000	0.014	0.029	0.043	0.021	0.021	0.007	0.007	0.021	0.043	0.029	0.029	0.072	0.065

WTC\FL	260	270	280	290	300	310	320	330	340	350	360	370	380	390	400
Heavy	0.046	0.028	0.039	0.050	0.051	0.064	0.055	0.081	0.072	0.090	0.041	0.027	0.010	0.008	0.000
Medium	0.022	0.024	0.026	0.033	0.040	0.050	0.050	0.080	0.083	0.125	0.087	0.046	0.019	0.010	0.002
Light	0.022	0.014	0.036	0.058	0.021	0.022	0.036	0.036	0.043	0.080	0.065	0.058	0.007	0.029	0.007

Table 16 PMF of temporary level-off FLs in descent for heavy, medium and light WTC

WTC\FL	100	110	120	130	140	150	160	170	180	190	200	210	220	230	240	250
Heavy	0.111	0.110	0.050	0.072	0.045	0.046	0.040	0.016	0.021	0.016	0.010	0.013	0.015	0.020	0.013	0.100
Medium	0.094	0.087	0.046	0.035	0.047	0.031	0.026	0.012	0.023	0.015	0.030	0.014	0.032	0.020	0.018	0.089
Light	0.113	0.098	0.036	0.011	0.018	0.025	0.025	0.018	0.051	0.040	0.036	0.051	0.033	0.030	0.040	0.076

WTC\FL	260	270	280	290	300	310	320	330	340	350	360	370	380	390	400
Heavy	0.062	0.004	0.011	0.012	0.017	0.043	0.020	0.024	0.020	0.046	0.017	0.019	0.005	0.002	0.000
Medium	0.035	0.012	0.057	0.030	0.046	0.048	0.042	0.017	0.025	0.029	0.028	0.008	0.004	0.001	0.000
Light	0.011	0.040	0.033	0.011	0.033	0.051	0.022	0.004	0.015	0.022	0.025	0.007	0.018	0.007	0.000

Table 17 PDF of air temperature near the ground (FL50) and lapse rate below the tropopause per season

Season	Air temperature	Lapse rate
Winter	Johnson SB (α=0.20, β=1.33, μ=258.60, k=27.95)	Johnson SB (α=0.39, β=1.15, μ=-8.24, k=4.85)
Spring	Johnson SB (α=0.61, β=1.03, μ=264.51, k=24.96)	Johnson SB (α=0.62, β=1.34, μ=-8.35, k=5.55)
Summer	Johnson SB (α=10.94, β=4.61, μ=262.38, k=223.06)	Johnson SB (α=2.18, β=2.13, μ=-8.66, k=7.94)
Autumn	Johnson SB (α=0.34, β=1.64, μ=258.37, k=40.76)	Johnson SB (α=0.97, β=1.32, μ=-8.10, k=5.30)
Year	Johnson SB (α=0.39, β=1.53, μ=257.72, k=41.50)	Johnson SB (α=0.89, β=1.39, μ=-8.28, k=5.60)

Table 18 PDF of a, b and c coefficients for u and v wind components' vertical profile estimation

		Winter	Spring	Summer	Autumn	Year
u	a	$U(0.00012, -0.00020)$	$U(0.00026, -0.00043)$	$U(-0.00018, 0.00014)$	$U(0.00013, -0.00025)$	$U(0.00007, -0.00017)$
	b	$U(-0.14119, 0.31885)$	$U(-0.22929, 0.37766)$	$U(-0.02660, 0.19089)$	$U(-0.19187, 0.34872)$	$U(-0.14471, 0.30639)$
	c	$U(-32.03890, 53.54877)$	$U(-25.98397, 25.32799)$	$U(-20.11592, 33.42056)$	$U(-32.88747, 34.11804)$	$U(-30.78149, 39.55576)$
v	a	$U(0.00020, -0.00023)$	$U(0.00057, -0.00069)$	$U(-0.00015, 0.00004)$	$U(0.00020, -0.00028)$	$U(0.00020, -0.00028)$
	b	$U(-0.36934, 0.28998)$	$U(-0.43345, 0.45717)$	$U(-0.20279, 0.23559)$	$U(-0.36048, 0.34620)$	$U(-0.34268, 0.33403)$
	c	$U(-19.61510, 26.25726)$	$U(-14.83457, 15.57422)$	$U(-14.18803, 16.47599)$	$U(-19.03989, 20.70540)$	$U(-17.21558, 20.02072)$

Table 19 PMF of ATC 'direct' instructions

Instruction	Direct-to	Direct-via
	0.808	0.192

Table 20 PMF of ATC heading instructions

Instruction	Present heading	Heading	Right turn	Left turn
	0.8615	0.1176	0.0105	0.0104

Table 21 PMF of ATC speed instruction types

Instruction	Assigned	Max	Min	Present speed
	0.502	0.256	0.241	0.001

Table 22 PMF of ATC instruction speed types

Instruction speed type	Mach	IAS
	0.697	0.303

Table 23 PMF of ATC Mach speed instruction

Mach	0.70	0.71	0.72	0.73	0.74	0.75	0.76	0.77	0.78	0.79	0.80	0.81	0.82	0.83	0.84	0.85	0.86
	0.002	0.002	0.006	0.009	0.084	0.170	0.138	0.103	0.198	0.121	0.055	0.039	0.040	0.018	0.008	0.005	0.002

Table 24 PMF of ATC IAS speed instruction

IAS, knots	260	270	280	290	300	310	320
	0.074	0.195	0.279	0.261	0.164	0.023	0.004

Table 25 PMF of ATC vertical speed (VS) instructions

VS instruction type	Descent rate	Climb rate
	0.834	0.166

Table 26 PMF of ATC vertical speed (VS) instruction limits

VS instruction limit	Minimum	Maximum
	0.994	0.006

Table 27 PMF of ATC rate of descent instruction

Rate of descent, feet/minute	-2500	-2000	-1500	-1000
	0.071	0.343	0.464	0.122

Table 28 PMF of ATC rate of climb instruction

Rate of climb, feet/minute	500	1000	1500	2000	2500
	0.030	0.508	0.392	0.067	0.003

Appendix B

Equations of the probability density functions are given below in alphabetical order.

A. Beta

The probability density function of the beta distribution is:

$$f(y, \alpha, \beta) = \frac{1}{k \cdot B(\alpha, \beta)} y^{\alpha-1}(1-y)^{\beta-1} \tag{15}$$

where $y = (x - \mu)/k$, μ is the location, k is the scale, α and β are the shape parameters, $\alpha > 0, \beta > 0$, and $B(\alpha, \beta)$ is defined with the gamma function Γ:

$$B(\alpha, \beta) = \frac{\Gamma(\alpha)\Gamma(\beta)}{\Gamma(\alpha + \beta)} \tag{16}$$

B. Exponential

The probability density function of the exponential distribution is:

$$f(y) = \frac{1}{k} \exp(-y) \tag{17}$$

where $y = (x - \mu)/k$, μ is the location, and k is the scale, $k > 0$.

C. Johnson SB

The probability density function of the Johnson SB distribution is:

$$f(y, \alpha, \beta) = \frac{\beta}{k \cdot y(1-y)} \phi\left(\alpha + \beta \log \frac{y}{1-y}\right) \tag{18}$$

where $y = (x - \mu)/k$, μ is the location, k is the scale, α and β are the shape parameters, $\alpha > 0, \beta > 0$, and ϕ is the probability density function of the standard normal distribution:

$$\phi(x) = \frac{1}{\sqrt{2\pi}} \exp(-x^2/2) \tag{19}$$

D. Johnson SU

The probability density function of the Johnson SU distribution is:

$$f(y, \alpha, \beta) = \frac{\beta}{k\sqrt{y^2 + 1}} \phi\left(\alpha + \beta \log\left(y + \sqrt{y^2 + 1}\right)\right) \tag{20}$$

where $y = (x - \mu)/k$, μ is the location, k is the scale, α and β are the shape parameters, $\alpha > 0, \beta > 0$, and ϕ is the probability density function of the standard normal distribution (Eq. (19)).

E. Log-Gamma

The probability density function of the log-gamma distribution is:

$$f(y, c) = \frac{\exp(c \cdot y - \exp(y))}{k \cdot \Gamma(c)} \tag{21}$$

where $y = (x - \mu)/k$, μ is the location, k is the scale, c is the shape parameter, $c > 0$, and Γ is the gamma function.

F. Mielke's Beta-Kappa

The probability density function of the Mielke's beta-kappa distribution is:

$$f(y, \lambda, s) = \frac{\lambda \cdot y^{\lambda-1}}{k \cdot (1 + y^s)^{1+\lambda/s}} \tag{22}$$

where $y = (x - \mu)/k$, μ is the location, k is the scale, λ and s are the shape parameters, $\lambda > 0$, $s > 0$.

G. Skew-normal

The probability density function of the skew-normal distribution is:

$$f(y, \alpha) = \frac{2}{k} \cdot \phi(y) \cdot \Phi(\alpha \cdot y) \tag{23}$$

where $y = (x - \mu)/k$, μ is the location, k is the scale, α is the skewness parameter, ϕ is the probability density function of the standard normal distribution (Eq. (19)) and Φ is the cumulative distribution function of the normal distribution:

$$\Phi(x) = \int_{-\infty}^{x} \phi(u) du \tag{24}$$

H. Uniform

The probability density function of the uniform distribution is:

$$f(x) = \frac{1}{b - a} \tag{25}$$

where a and b are the minimum and maximum values of the support, $x \in [a, b]$.

References

[1] ICAO, *TBO Concept. Appendix A to WP652 TBOCD 3.0*, 2015.

[2] EUROCONTROL, *European ATM Master Plan*, 2015.

[3] Musialek, B., Munafo, C. F., Ryan, H., and Paglione, M., "Literature survey of trajectory predictor technology," Tech. Rep. DOT/FAA/TC-TN11/1, Federal Aviation Administration, 2010.

[4] Mondoloni, S., *Aircraft Trajectory Prediction Errors: Including a Summary of Error Sources and Data*, Version 0.2 ed., 2006.

[5] Mondoloni, S., Paglione, M., and Green, S. M., "Trajectory modelling accuracy for air traffic management decision support tools," *International Congress of Aeronautical Sciences*, 2002.

[6] Gerretsen, A., and Swierstra, S., "Sensitivity of aircraft performance to Variability of input data," Tech. Rep. DOC CoE-TP-02005, EUROCONTROL, 2003.

[7] Swierstra, S., and Green, S. M., "Common trajectory prediction capability for decision support tools," *5th USA/Europe ATM R&D Seminar*, Budapest, Hungary, 2003.

[8] Mondoloni, S., and Bayraktutar, I., "Impact of factors, conditions and metrics on trajectory prediction accuracy," *6th USA/Europe ATM R&D Seminar*, Baltimore, MD, 2005.

[9] Paglione, M., Bayraktutar, I., Mcdonald, G., and Bronsvoort, J., "Lateral Intent Error's Impact on Aircraft Prediction," *8th USA/Europe ATM R&D Seminar*, Napa, CA, 2009.

[10] Torres, S., "Determination and ranking of trajectory accuracy factors," *IEEE/AIAA 29th Digital Avionics Systems Conference*, Salt Lake City, UT, 2010.

[11] Bronsvoort, J., "Contributions to trajectory prediction theory and its application to arrival management for air traffic control," Ph.D. thesis, Universidad Politécnica de Madrid, 2014.

[12] Nuic, A., *User Manual for the Base of Aircraft Data (BADA) Revision 3.12*, EEC Technical/Scientific Report No. 14/04/24-44 ed., 2014.

[13] The Boeing Company, *737-600/-700/-800/-900. Flight Crew Operations Manual*, D6-27370-TBC. Revision 21 ed., 2008.

[14] Glover, W., and Lygeros, J., "A Multi-Aircraft Model for Conflict Detection and Resolution Algorithm Evaluation," Tech. rep., HYBRIDGE, IST-2001-32460 Work Package WP1, Deliverable D1.3 A, 2004.

[15] Camilleri, W., Chircop, K., Zammit-Mangion, D., Sabatini, R., and Sethi, V., "Design and Validation of a Detailed Aircraft Performance Model for Trajectory Optimization," *AIAA Modeling and Simulation Technologies Conference*, Minneapolis, MN, 2012. doi:10.2514/6.2012-4566.

[16] Lee, A. G., Wu, M. G., and Abramson, M., "Modeling of Complex and Diverse Aircraft Trajectories with the Trajectory Synthesizer Generalized Profile Interface," *AIAA Modeling and Simulation Technologies Conference*, Kissimmee, FL, 2015.

[17] Sun, J., Ellerbroek, J., and Hoekstra, J., "Modeling Aircraft Performance Parameters with Open ADS-B Data," *12th USA/Europe ATM R&D Seminar*, Seattle, WA, 2017.

[18] Slater, G., "Study on variations in vertical profile for CDA descents," *9th AIAA Aviation Technology, Integration, and Operations Conference (ATIO)*, Hilton Head, SC, 2009. doi:10.2514/6.2009-6912.

[19] Torres, S., Dehn, J., Mckay, E., Paglione, M. M., and Schnitzer, B. S., "En-route Automation Modernization (ERAM) trajectory model evolution to support trajectory-based operations (TBO)," *IEEE/AIAA 34th Digital Avionics Systems Conference*, Prague, Czech Republic, 2015.

[20] McConkey, E. D., and Bolz, E. H., "Analysis of the Vertical Accuracy of the CTAS Trajectory Prediction Process," Tech. rep., Science Applications International Corporation, Arlington, Virginia, 2002.

[21] Alligier, R., Gianazza, D., and Durand, N., "Ground-based Estimation of the Aircraft Mass, Adaptive vs. Least Squares Method," *10th USA/Europe ATM R&D Seminar*, Chicago, IL, 2013.

[22] Casado Magaña, E. J., "Trajectory prediction uncertainty modelling for Air Traffic Management," Ph.D. thesis, University of Glasgow, 2016.

[23] Casado, E., D'Alto, L. P., and Vilaplana, M., "Analysis of the Impact of Intent Uncertainty on the Accuracy of Predicted Trajectories for Arrival Management Automation," *6th International Conference on Research in Air Transportation*, 2014.

[24] Suchkov, A., Swierstra, S., and Nuic, A., "Aircraft Performance Modelling for Air Traffic Management Applications," *5th USA/Europe ATM R&D Seminar*, Budapest, Hungary, 2003.

[25] Jones, T., Rustenburg, J. W., Skinn, D. A., Tipps, D. O., and DeFiore, T., "Statistical data for the Boeing-747-400 aircraft in commercial operations," Tech. Rep. DOT/FAA/AR-04/44, Federal Aviation Administration, 2005.

[26] EUROCONTROL, *Vertical flight efficiency*, 2008. Final report.

[27] Roach, K., and Robinson, J. E., "A Terminal Area Analysis of Continuous Ascent Departure Fuel Use at Dallas/Fort Worth International Airport," *AIAA Aircraft Technology, Integration,and Operations (ATIO)*, Fort Worth, TX, 2010. doi: 10.2514/6.2010-9379.

[28] Miller, M. E., Graham, M., and Aldous, J., "Efficient climb and descent benefit pool," *IEEE/AIAA 30th Digital Avionics Systems Conference*, 2011. doi:10.1109/DASC.2011.6096003.

[29] ICAO, *Manual of the ICAO Standard Atmosphere extended to 80 kilometres (262,500 feet)*, 1993.

[30] Smith, M. S., "A New Tool for Estimating Atmospheric Conditions in Four Dimensions," *AIAA Balloon Systems Conference*, Denver, CO, 2017. doi:10.2514/6.2017-3285.

[31] Porretta, M., Dupuy, M.-D., Schuster, W., Majumdar, A., and Ochieng, W., "Performance Evaluation of a Novel 4D Trajectory Prediction Model for Civil Aircraft," *Journal of Navigation*, Vol. 61, No. 3, 2008, pp. 393–420. doi:10.1017/S0373463308004761.

[32] Lymperopoulos, I., and Lygeros, J., "Sequential Monte Carlo methods for multi-aircraft trajectory prediction in air traffic management," *Int. J. Adapt. Control Signal Process*, Vol. 24, 2010, pp. 830–849. doi:10.1002/acs.1174.

[33] Gallo, E., "Prediction of descent trajectories based on aircraft intent," *IEEE/AIAA 29th Digital Avionics Systems Conference*, Seattle, WA, 2010. doi:10.1109/DASC.2010.5655487.

[34] Hernandez, E., Valenzuela, A., and Rivas, D., "Probabilistic Aircraft Conflict Detection Considering Ensemble Weather Forecast," *6th SESAR Innovation Days*, 2016.

[35] Kim, J., Palaniappan, K., Menon, P. K., Nag, M., and Subbarao, K., "Trajectory Uncertainty Modeling for Queueing Analysis of the NAS," *26th Congress of International Council of the Aeronautical Sciences (ICAS)*, Anchorage, AK, 2008. doi:10.2514/6.2008-8854.

[36] Robert, E., and De Smedt, D., "Comparison of operational wind forecasts with recorded flight data," *10th USA/Europe ATM R&D Seminar*, Chicago, IL, 2013.

[37] Aldrich, J., "R. A. Fisher and the Making of Maximum Likelihood 1912-1922," *Statistical Science*, Vol. 12, No. 3, 1997, pp. 162–176.

[38] Massey, F. J. J., "The Kolmogorov-Smirnov test for goodness of fit," *Journal of the American Statistical Association*, Vol. 46, No. 253, 1951, pp. 68–78.

[39] Parzen, E., "On estimation of a probability density function and mode," *The Annals of Mathematical Statistics*, Vol. 33, 1962, pp. 1065–1076.

[40] Silverman, B., "Density estimation for statistics and data analysis," *Monographs on Statistics and Applied Probability*, Vol. 26, 1986.

[41] Savitzky, A., and Golay, M. J. E., "Smoothing and Differentiation of Data by Simplified Least Squares Procedures," *Analytical Chemistry*, Vol. 36, No. 8, 1964, pp. 1627–1639. doi:10.1021/ac60214a047.

[42] EUROCONTROL, *Surveillance Data Exchange. Part 9: Category 062. SDPS Track Messages*, 2010.

[43] Carta, J. A., Ramírez, P., and Velázquez, S., "A review of wind speed probability distributions used in wind energy analysis. Case studies in the Canary Islands," *Renewable and Sustainable Energy Reviews*, Vol. 13, 2009, pp. 933–955. doi:10.1016/j.rser.2008.05.005.

[44] Monahan, A. H., He, Y., McFarlane, N., and Dai, A., "The Probability Distribution of Land Surface Wind Speeds," *Journal of climate*, Vol. 24, 2011, pp. 3892 – 3909. doi:10.1175/2011JCLI4106.1.

[45] Carrillo, C., Cidrás, J., Díaz-Dorado, E., and Obando-Montaño, A. F., "An Approach to Determine the Weibull Parameters for Wind Energy Analysis: The Case of Galicia (Spain)," *Energies*, Vol. 7, 2014, pp. 2676–2700. doi:10.3390/en7042676.

[46] Kamisan, N. A. B., Hussin, A. G., Zubairi, Y. Z., and Hassan, S. F., "Distribution of wind direction recorded at maximum wind speed: A case study of Malaysian wind data for 2005," *International Journal of the Physical Sciences*, Vol. 6, No. 7, 2011, pp. 1840–1850.

[47] Heckenbergerová, J., Musilek, P., Mejznar, J., and Vančura, M., "Estimation of wind direction distribution with genetic algorithms," *26th IEEE Canadian Conference Of Electrical And Computer Engineering*, 2013.